Mammalian Muscle Model for Predicting Force and Energetics During Physiological Behaviors

George A. Tsianos, Cedric Rustin, and Gerald E. Loeb, *Member, IEEE*

***Abstract*—Muscles convert metabolic energy into mechanical work. A computational model of muscle would ideally compute both effects efficiently for the entire range of muscle activation and kinematic conditions (force and length). We have extended the original Virtual Muscle algorithm (Cheng *et al.*, 2000) to predict energy consumption for both slow- and fast-twitch muscle fiber types, partitioned according to the activation process ($\mathbf{E_a}$), cross-bridge cycling ($\mathbf{E_{xb}}$) and ATP/PCr recovery ($\mathbf{E_{recovery}}$). Because the terms of these functions correspond to identifiable physiological processes, their coefficients can be estimated directly from the types of experiments that are usually performed and extrapolated to dynamic conditions of natural motor behaviors. We also implemented a new approach to lumped modeling of the gradually recruited and frequency modulated motor units comprising each fiber type, which greatly reduced computational time. The emergent behavior of the model has significant implications for studies of optimal motor control and development of rehabilitation strategies because its trends were quite different from traditional estimates of energy (e.g., activation, force, stress, work, etc.). The model system was scaled to represent three different human experimental paradigms in which muscle heat was measured during voluntary exercise; predicted and observed energy rate agreed well both qualitatively and quantitatively.**

***Index Terms*—Energetics, modeling, muscle, recruitment.**

I. Introduction

OPTIMIZATION methods have long been used to find unique solutions for the performance of tasks by "over-complete" musculoskeletal systems [2]–[4]. Similarly, optimal control theory can be used to adjust gains in feedback systems [5]–[7]. The physiological soundness of the strategies identified with these tools depends on defining performance criteria that are relevant to the task and the organism. Metabolic energy consumption is a teleologically appealing criterion and there are empirical data supporting it for locomotion and reaching [8], [9], but it is difficult to measure or model at the individual muscle level. Instead, cost functions usually include estimates of muscle recruitment, stress or work that may differ greatly from energy consumption depending on factors such as sarcomere velocity and fiber type.

Manuscript received March 14, 2011; revised June 10, 2011; accepted June 13, 2011. Date of publication August 18, 2011; date of current version March 16, 2012. This work was supported in part by the DARPA REPAIR Program and the Myronis Fellowship Foundation.

G. A. Tsianos is with the Biomedical Engineering Department, University of Southern California, Los Angeles, CA 90089 USA (e-mail: tsianos@usc.edu).

C. Rustin is with the Theoretical Mechanics Department, University of Mons, B7000 Mons, Belgium (e-mail: cedric.rustin@umons.ac.be).

G. E. Loeb is with the Biomedical Engineering Department, University of Southern California, Los Angeles, CA 90089 USA (e-mail: gloeb@usc.edu).

Digital Object Identifier 10.1109/TNSRE.2011.2162851

Some cost functions have included models of muscle energetics that are more consistent with metabolic cost [10]–[12]. They are based primarily on the heat output rate and power measurements under various conditions of stimulation that together mirror metabolic energy consumption [13]. The main issues with these models is that they rely almost entirely on enthalpy data, which are sparse, at least partly based on nonmammalian species and do not reflect the true energetic cost under many conditions. Energetic data on submaximally stimulated, lengthening muscle are especially limited for mammals, so modelers often resort to data from nonmammalian species. There is even a discrepancy between enthalpy data presented by Barclay *et al.*, 1993 [14] and Barclay, 1996 [15] for shortening, tetanically stimulated mouse muscle, as discussed by Houdijk *et al.* [16]. Umberger [12] developed a model of muscle energetics based on Barclay *et al.*, 1993, which Houdijk *et al.* found was internally inconsistent with mechanical work. Houdijk *et al.* found that enthalpy and efficiency estimates from Hatze and Buys' earlier model [17] were in qualitative agreement with data from Barclay, 1996, which we have used as part of the thermodynamic basis for our model.

Models based on enthalpy experiments estimate the energetics of lengthening muscle poorly. This is because during eccentric contractions substantial mechanical energy is stored through various mechanisms such as tendon, aponeurosis, parallel elastic element and cross bridge compliance [18]–[21], and perhaps also through changes in cross-bridge biochemical state [19], [22]. The negative work done on the muscle cannot be stored indefinitely nor can it be converted back into chemical energy. The absorbed energy is not released until after the lengthening phase, however, which creates a large discrepancy between the enthalpy measured and the metabolic energy consumed during activation under lengthening conditions. Many models use this enthalpy data, assuming it is equivalent to metabolic cost and therefore make inaccurate predictions for the energetics.

Estimating muscle activation using classical Hill-type models also leads to significant inaccuracies in both energetic cost and force production. These models generally do not capture the dependence of activation on length and fiber specific properties such as sag and yield [23], [24]. These effects are particularly strong at physiological firing rates, as opposed to the tetanic frequencies at which experiments are often conducted.

Sag refers to the phenomenon in which the force produced by an isometric muscle in response to a constant frequency of stimulation initially rises to a peak value and then declines slowly [24]. This is thought to occur due to calcium-mediated increase in the rate of calcium reuptake, which reduces calcium ion concentration in the sarcoplasm, hence the number

of available binding sites. It occurs primarily in fast-twitch muscle and presumably contributes to speed of relaxation. Given this mechanism, the effects of sag reflect a decrease in the number of cross-bridges and therefore should be included in the energetics model.

Yielding is the phenomenon associated with the dependence of the force-velocity relationship on stimulation frequency [25], or conversely the tendency for a given isometric force to decrease if the active muscle is then stretched or shortened at even moderate velocities. It occurs primarily in slow-twitch fibers where the rate of cross-bridge reattachment appears to be a limiting step [23]. Yielding is more pronounced at submaximal activations, perhaps because the limiting factor in attachment rate is related to the stereochemical alignment between the myosin head and exposed cross-bridge binding sites on the helical actin. When all binding sites are available at full activation, a cross-bridge that detaches due to motion is more likely to reattach rapidly and the force will be maintained. At reduced activation, more of the available binding sites will be suboptimally oriented. If slow-twitch myosin is less mobile or slower to attach than fast-twitch myosin, then rate of reattachment might become the limiting step in cross-bridge cycling and, hence, energy consumption. The correlation of yield to muscle stiffness [26] provides further support for a mechanism related to the number of cross-bridges formed.

The validity of models that are based on empirical data depends on the accuracy and richness of the dataset used, neither of which is really satisfactory for muscle energetics. We have used most of the available enthalpy data from mammalian muscle in a model whose structure is closely related to the individual physiological processes underlying activation, force production and energy consumption. This improves the likelihood that the model can be interpolated and extrapolated to predict energy consumption for conditions that have not been studied, and it provides a straightforward mechanism to test its validity and to improve its parameter estimation as new data become available.

II. Methods

A. Model Design and Rationale

The energetics of muscle contraction can be separated into an initial component $(\mathrm{E_{initial}})$ that is consumed in phase with the contraction and a recovery component $(\mathrm{E_{recovery}})$ that lags the contraction slightly and lasts up to a few minutes following its termination [27]. $\mathrm{E_{initial}}$ corresponds to the ATP consumed at the time of the contraction and its rapid replenishment through the creatine kinase reaction [13]. $\mathrm{E_{recovery}}$ corresponds mainly to the energy consumed by metabolic pathways for restoring ATP and phosphocreatine (PCr) concentration in the sarcoplasm. The energy supplied from ATP molecules fuels two main processes during the contraction: regulating concentration gradients of ions that excite the muscle fiber and its contractile machinery $(\mathrm{E_a})$ and cycling of cross-bridges that generate contractile force $(\mathrm{E_{xb}})$. Partitioning energetics among these physiological processes in the model is important for computing energy consumption for untested conditions because it allows us to extrapolate their contributions independently according to the specific stimulation parameters that affect them.

1) Energy Consumption Related to Cross-Bridge Cycling: The majority of the energy supplied by ATP is consumed due to cross-bridge cycling and is referred to as cross-bridge energy $(\mathrm{E_{xb}})$. For a cross-bridge to form, myosin heads must be in a high-energy, strained configuration containing bound ADP. Such myosin heads bind rapidly to nearby actin sites that are exposed by calcium activation. The elastic energy stored in the myosin head is subsequently released depending on the external load on the cross-bridge. If the load is less than the restoring force of the cross-bridge, then the myosin head will move "concentrically," reducing its contribution to contractile force toward zero at its equilibrium position, where it has the highest probability of detachment from the actin site. The detachment process is coupled to recocking of the head in the strained configuration, which requires a fresh ATP molecule to displace the ADP. If the load is greater than the restoring force of the attached cross-bridges, the muscle fiber will lengthen, pulling the cross-bridges to even greater strain angles where forces increase but then drop as the cross-bridges are forcibly detached. This "eccentric" detachment leaves the myosin heads in their cocked state, so they can immediately reattach to an available binding site without consuming energy (although the actual rate of reattachment may depend on the relative availability of binding sites, which in turn depends on the level of activation; see description of yielding phenomenon in the Introduction). The amount of energy consumed by muscle due to cross-bridge cycling therefore depends on how many cross-bridges are attached and the rate at which they are cycling concentrically, as opposed to the amount of force that they are generating. The number of cross-bridges formed depends primarily on firing rate, myofilament overlap, and the effects of sag and yield (see Introduction). Cycling rate depends mainly on the velocity of contraction as measured at the muscle fiber, but it does not fall to zero for so-called isometric contractions. This could arise from substantial "squirming motion" of the myofilaments due to their compliance, the pulsatile excitation of muscle fibers, the stochastic distribution of cross-bridges at any instant, and/or thermal vibration of all of the molecular structures.

2) Energy Consumption Related to Excitation: The energy associated with ionic excitation is typically referred to as activation energy $(\mathrm{E_a})$ and is related to the number of ATP molecules consumed by membrane-bound pumps for sodium, potassium and calcium ions. When an excitatory impulse from a motoneuron is transmitted through the neuromuscular junction and spreads along the muscle fiber and into the transverse tubules, it depends on sodium and potassium ions leaking across the cell membrane down electrochemical gradients. These electrochemical gradients must then be maintained through the Na+-K+ pump at the expense of ATP to allow transmission of subsequent impulses. Action potentials at the points of contact between the transverse tubules and cisternae of the sarcoplasmic reticulum (SR) lead to release of calcium ions from the cisternae down their concentration gradient into the sarcoplasm, where they bind to troponin and induce a conformation change along the thin filament that exposes

binding sites for cross-bridges. To regulate calcium flux within the sarcoplasm and restore the calcium concentration gradient, additional ATP is expended to pump calcium back into the SR, allowing the muscle to relax and restoring calcium to the cisternae. The component of E_a that is related to action potentials along the sarcolemma is small and generally proportional to the firing rate of the motor unit. The component of E_a that is related to calcium activation of cross-bridge binding is larger and initially proportional to firing rate but tends to plateau at higher frequencies because of temporary depletion of calcium in the cisternae [28].

3) Recovery Energy: The recovery energy is the energy required to restore the ATP and PCr concentrations in the sarcoplasm. ATP can be synthesized via aerobic or anaerobic metabolic pathways, after which it may react with creatine to form PCr. Muscle undergoes anaerobic metabolism when oxygen levels are insufficient for oxidative pathways, which tends to occur during sustained, strong contractions of muscles that generate hydrostatic pressures sufficient to occlude capillary blood flow. These metabolic pathways have different efficiencies, meaning that they consume different amounts energy per ATP or PCr molecule synthesized. The total energy consumed in this phase, therefore, depends on the amount of ATP and PCr needed to be restored and on the specific metabolic pathways involved. Fast-twitch muscle fibers (type IIb) have a low oxidative capacity but large amounts of stored glycogen, which they can metabolize anaerobically, albeit inefficiently, to replenish ATP during strong contractions. Slow-twitch (and type IIa fast-twitch fibers) muscles have little stored glycogen but they have a high oxidative capacity to restore ATP efficiently from the complete oxidation of glucose absorbed from blood flow.

B. Implementation of the Model

In thermodynamic experiments, the sum of heat and work measured during isovelocity contractions and isometric contractions of brief duration reflects $E_{initial}$. The heat that is produced largely after the contraction is referred to as recovery heat and corresponds to $E_{recovery}$ (see [27], [29]–[31]).

The model for $E_{initial}$ is based on thermodynamic data characterizing the relationship of energy to shortening velocity [15] for both slow- and fast-twitch muscle and division into contributions from E_{xb} and E_a [32], [33]. The data, however, are obtained mostly from tetanically stimulated muscle at optimal sarcomere length. Virtual Muscle (VM) [1] incorporates models of processes such as gradual recruitment and frequency modulation of different muscle fiber types and their interaction with force-length and force-velocity relationships for those fiber types. Thus the addition of an energetics model required estimation of coefficients to rescale existing terms for excitation (firing rates) and force generation (newtons, N) into units of energy consumption per unit time (watts, W). We also redesigned a continuous recruitment algorithm for VM based on the lumped motor unit scheme presented in [34], so that it is both computationally efficient and able to provide accurate estimates of both muscle energetics and force in muscles with various mixtures of two different fiber types (see Appendix A). The model and its implementation depend on certain assumptions.

1) All mammalian skeletal muscles use similar chemical pathways and molecular mechanisms to convert metabolic energy into mechanical work, thereby allowing us to pool data from different species.
2) The energy cost of all physiological processes is a function of ATP regenerated to restore the initial conditions, which is not related strictly to the chemical or mechanical work performed or heat liberated when that work was performed.
3) Processes related to ATP regeneration occur mostly within the contracting muscle rather than in other organs (e.g., liver) that are involved in metabolism, therefore, enthalpy measurements from isolated muscle preparations are good approximations of energy cost.
4) The metabolic cost of ATP regeneration via a given chemical pathway is independent of operating temperature [13], thereby allowing us to utilize data from preparations typically below normal body temperature to preserve their viability. The actual energy required to drive a given chemical reaction (e.g., regeneration of ATP from PCr) is a function of temperature, but the energy available in the biological source (PCr) is higher than that by a safety margin. As long as the reaction takes place at all, the total energy consumed will be constant and equal to the sum of chemical energy stored in any products (e.g., ATP) plus excess energy dissipated as heat and/or work.

The energetics algorithm (refer to the block diagram in Fig. 1) is divided into sections that correspond to the major physiological processes underlying energy consumption. Equations for terms used in the energetics algorithm are defined in Table I and their corresponding symbols are defined in Table II (see Appendix A for more details on their derivation). The sequence and specific form of the computations was determined by the experimental data that were available. E_a, for example, has been investigated relative to E_{xb} rather than as an explicit function of firing rate, so in order to calculate its contribution to total energy expenditure for submaximal stimulation, we computed E_{xb} in absolute units first. Similarly, $E_{recovery}$ is defined in the literature as a multiple of $E_{initial}$ so we had to compute $E_{initial}$ first to obtain $E_{recovery}$.

1) Energy Consumption Related to Cross-bridge Cycling: To extract the contribution of cross-bridge cycling from the $E_{initial}$-velocity relationships presented in [15] for tetanically stimulated muscle at optimal sarcomere length, we calculated the contribution of E_a based on the finding from [32], [33] that it is approximately one third (parameter "a" in the model) of the initial energy consumed in the isometric condition (Fig. 1, STEP 1)

$$E_a(f = f_{tet}) = a * E_{initial}(f = f_{tet}, L_{ce} = L_{ce0}, V_{ce} = 0).$$

Note: $E_{initial}$ differs significantly for each fiber type and was therefore handled separately in the model.

Because E_a is assumed independent of contractile velocity, we removed this value from the entire $E_{initial}$-velocity relationship to obtain the shortening E_{xb}-velocity relationship for tetan-

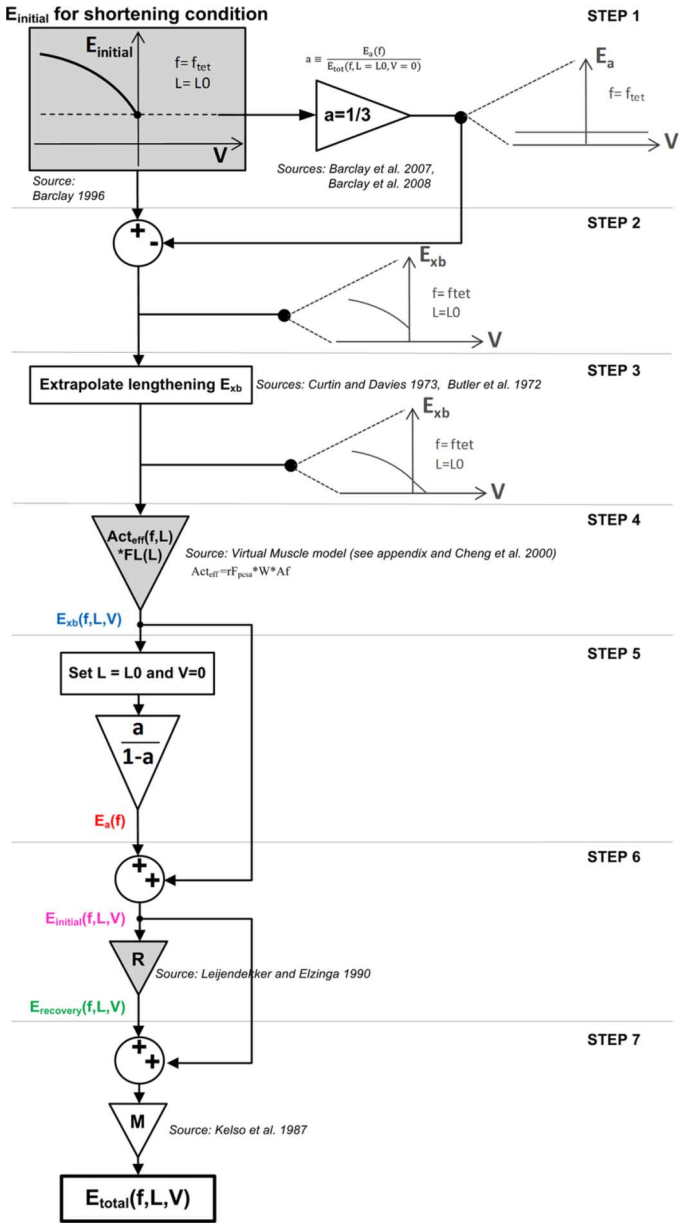

Fig. 1. Overview of the energetics algorithm. Thermodynamic data for tetanically stimulated muscle at optimal sarcomere length provide the basis for the energetics model. Data from force production experiments that characterize underlying physiological processes were used to generalize the model across a wide range of firing rates and sarcomere kinematics. Gray elements in the diagram are dependent on fiber type. See text for details.

ically stimulated muscle at optimal sarcomere length (Fig. 1, STEP 2)

$$\begin{aligned}\mathrm{E_{xb}}(\mathrm{f}=\mathrm{f_{tet}},\mathrm{L_{ce}}=\mathrm{L_{ce0}},\mathrm{V_{ce}}\le 0)\\ =\mathrm{E_{initial}}(\mathrm{f}=\mathrm{f_{tet}},\mathrm{L_{ce}}=\mathrm{L_{ce0}},\mathrm{V_{ce}}\le 0)-\mathrm{E_a}(\mathrm{f}=\mathrm{f_{tet}}).\end{aligned}$$

The $\mathrm{E_{xb}}$-velocity relationship for lengthening muscle was designed to capture the observation that ATP consumption rate in actively lengthening muscle decreases to a low steady level near zero at a modest lengthening velocity (see [35] and [36]). Because the energy over this range of velocities is relatively small and constant, it can be assumed that it corresponds almost entirely to $\mathrm{E_a}$ (i.e., $\mathrm{E_{xb}}=0$). Thus, we computed the energy rate due to cross-bridge cycling by linearly extrapolating the shortening $\mathrm{E_{xb}}$-velocity relationship from the isometric condition down to zero energy. $\mathrm{E_{xb}}$ was set to zero for larger lengthening velocities (Fig. 1, STEP 3)

$$\begin{aligned}&\mathrm{E_{xb}}(\mathrm{f}=\mathrm{f_{tet}},\mathrm{L_{ce}}=\mathrm{L_{ce0}},\mathrm{V_{ce}}>0)\\ &\quad=\Big[\mathrm{E_{xb}}(\mathrm{f}=\mathrm{f_{tet}},\mathrm{L_{ce}}=\mathrm{L_{ce0}},\mathrm{V_{ce}}=0)\\ &\qquad+\frac{\mathrm{d}}{\mathrm{dV}}[\mathrm{E_{xb}}(\mathrm{f}=\mathrm{f_{tet}},\mathrm{L_{ce}}=\mathrm{L_{ce0}},\mathrm{V_{ce}})]\big|_{\mathrm{V_{ce}}=0}*\mathrm{V_{ce}}\Big]\\ &\qquad*\mathrm{if}(\mathrm{E_{xb}}\ge 0).\end{aligned}$$

Note that the linear approximation has negligible effects on the model's accuracy for most behavioral tasks, as $\mathrm{E_{xb}}$ during lengthening has a relatively small contribution to the overall energetic cost.

To obtain $\mathrm{E_{xb}}$ for physiological firing rates and kinematics, we scaled this relationship with the $\mathrm{Act_{eff}}$ $(=\mathrm{rFpcsa}*\mathrm{W}*\mathrm{Af})$, and FL terms in VM (see Appendix A), which provide a measure of the number of cross-bridges formed depending on these conditions (Fig. 1, STEP 4)

$$\begin{aligned}\mathrm{E_{xb}}(\mathrm{f},\mathrm{L_{ce}},\mathrm{V_{ce}})=\mathrm{Act_{eff}}(\mathrm{f},\mathrm{L_{ce}})*\mathrm{FL}(\mathrm{L_{ce}})\\ *\mathrm{E_{xb}}(\mathrm{f}=\mathrm{f_{tet}},\mathrm{L_{ce}}=\mathrm{L_{ce0}},\mathrm{V_{ce}}).\end{aligned}$$

Note: Acteff and FL are different for each fiber type due to type-specific biochemical and mechanical properties of the contractile machinery. The sag phenomenon in fast-twitch fibers and yield in slow-twitch fibers, for example, are incorporated into the model through the Af term of VM (see [24] and [25] for more details on modeling of sag and yield, respectively). The role of these terms in VM's energetics and force models is shown schematically in Fig. 10 (see Appendix A for an overview of VM).

2) Energy Consumption Related to Excitation: Researchers typically study $\mathrm{E_a}$ relative to $\mathrm{E_{initial}}$ or $\mathrm{E_{xb}}$ rather than as an explicit function of firing rate, so we scaled $\mathrm{E_{xb}}$ to calculate its contribution to total energy expenditure. To measure $\mathrm{E_a}$ in intact muscle, experimentalists record the heat output of muscle stimulated isometrically under conditions that prevent cross-bridge formation. This can be done mechanically by stretching the muscle so as to eliminate myolfilament overlap or pharmacologically by exposure to BTS (N-benzyl-p-toluenesulphonamide) to inhibit the binding of myosin heads to actin sites [32], [33]. Both techniques produce similar results for slow- and fast-twitch mammalian muscle at temperatures within the range of 20 °C to 30 °C. It has been shown that the energy expended by excitation is roughly one third of $\mathrm{E_{initial}}$ consumed by muscle that is contracting isometrically at optimal sarcomere length. Equivalently, the activation energy consumed is one half of the energy consumed due to cross-bridge cycling (given that $\mathrm{E_{initial}}=\mathrm{E_{xb}}+\mathrm{E_a}$ and $\mathrm{a}=1/3$; Fig. 1, STEP 5)

$$\mathrm{E_a}(\mathrm{f})=\frac{\mathrm{a}}{1-\mathrm{a}}*\mathrm{E_{xb}}(\mathrm{f},\mathrm{L_{ce}}=\mathrm{L_{ce0}},\mathrm{V_{ce}}=0).$$

3) Recovery Energy: The enthalpy resulting from ATP and PCr resynthesis is naturally related to the ATP and PCr ex-

TABLE I
TABLE OF EQUATIONS

Equations	Slow-twitch fibers				Fast-twitch fibers			
$\bar{F}_{se}(\bar{L}_{se}) = c^T k^T \ln\left\{\exp\left[\frac{\bar{L}_{se} - L_r^T}{k^T}\right] + 1\right\}$	c^T	k^T	L_r^T		c^T	k^T	L_r^T	
	27.8	.0047	0.964		27.8	.0047	0.964	
$\bar{F}_{pe1}(\bar{L}_{ce}, \bar{V}_{ce}) = c_1 k_1 \ln\left\{\exp\left[\frac{\bar{L}_{ce}/\bar{L}_{ce}^{\max} - L_{r1}}{k_1}\right] + 1\right\} + \eta \bar{V}_{ce}$	c_1	k_1	L_{r1}	η	c_1	k_1	L_{r1}	
	23.0	0.046	1.17	0.01	23.0	0.046	1.17	
$\bar{F}_{pe2}(\bar{L}_{ce}) = c_2\{\exp[k_2(\bar{L}_{ce} - L_{r2})]\} - 1\}, \quad \bar{F}_{pe2} \le 0$	c_2	k_2	L_{r2}		c_2	k_2	L_{r2}	
	−0.02	−21.0	0.70		−0.02	−21.0	0.70	
$FL(\bar{L}_{ce}) = exp\left(-\left\lvert\frac{\bar{L}_{ce}^{\beta} - 1}{\omega}\right\rvert^{\rho}\right)$	ω	β	ρ		ω	β	ρ	
	1.12	2.30	1.62		0.75	1.55	2.12	
$FV(\bar{V}_{ce}, \bar{L}_{ce}) =$	$V_{\max}$	c_{v0}	c_{v1}		$V_{\max}$	c_{v0}	c_{v1}	
$\begin{cases} (V_{\max} - \bar{V}_{ce})/[V_{\max} + (c_{v0} + c_{v1}\bar{L}_{ce})\bar{V}_{ce}], & \bar{V}_{ce} \le 0 \\ [b_v - (a_{v0} + a_{v1}\bar{L}_{ce} + a_{v2}\bar{L}_{ce}^2)\bar{V}_{ce}]/(b_v + \bar{V}_{ce}), & \bar{V}_{ce} > 0 \end{cases}$	−7.88	5.88	0		−9.15	−5.70	9.18	
	a_{v0}	a_{v1}	a_{v2}	b_v	a_{v0}	a_{v1}	a_{v2}	b_v
	−4.70	8.41	−5.34	0.35	−1.53	0	0	0.69
$Af^{slow}(f_{eff}, \bar{L}_{ce}, \bar{V}_{ce}) = 1 - \exp\left[-\left(\frac{Yf_{eff}}{a_f n_f}\right)^{n_f}\right]$								
$Af^{fast}(f_{eff}, \bar{L}_{ce}) = 1 - \exp\left[-\left(\frac{Sf_{eff}}{a_f n_f}\right)^{n_f}\right]$	a_f	n_{f0}	n_{f1}		a_f	n_{f0}	n_{f1}	
	0.56	2.1	5		0.56	2.1	3.3	
$n_f = n_{f0} + n_{f1}\left(\frac{1}{\bar{L}_{ce}} - 1\right)$								
$\dot{Y}(t) = \frac{1 - c_Y\left[1 - exp\left(-\frac{\lvert\bar{V}_{ce}\rvert}{V_Y}\right)\right] - Y(t)}{T_Y}$	c_Y	V_Y	$T_Y(ms)$		–	–	–	
	0.35	0.1	200					
$\dot{S}(t, f_{eff}) = \frac{a_S - S(t)}{T_S}, \quad a_S = \begin{cases} a_{S1}, f_{eff}(t) < 0.1 \\ a_{S2}, f_{eff}(t) \ge 0.1 \end{cases}$	–	–	–		a_{S1}	a_{S2}	$T_S(ms)$	
					1.76	0.96	43	
$\dot{f}_{int}(t, f_{env}, \bar{L}_{ce}) = \frac{f_{env}(t) - f_{int}(t)}{T_f}, \quad T_f = \begin{cases} T_{f1}\bar{L}_{ce}^2 + T_{f2} f_{env}(t), \dot{f}_{eff} \ge 0 \\ (T_{f3} + T_{f4} Af)/\bar{L}_{ce}, \dot{f}_{eff} < 0 \end{cases}$								
$\dot{f}_{eff}(t, f_{int}, \bar{L}_{ce}) = \frac{f_{int}(t) - f_{eff}(t)}{T_f}$	$T_{f1}(ms)$	$T_{f2}(ms)$	$T_{f3}(ms)$	$T_{f4}(ms)$	$T_{f1}(ms)$	$T_{f2}(ms)$	$T_{f3}(ms)$	$T_{f4}(ms)$
	34.3	22.7	47.0	25.2	20.6	13.6	28.2	15.1
$\dot{U}_{eff} = \frac{U - U_{eff}}{T_U}, \quad T_U = \begin{cases} T_{rise} e^{-(U - U_{eff})\ln(1000 T_{rise})} & U \ge U_{eff} \\ T_{fall} & U < U_{eff} \end{cases}$	$T_{rise} = 0.38 U_{th}^{fast\,2} + 0.8 U_{th}^{fast} + 0.14$							
	$T_{fall} = -0.32 U_{th}^{fast\,4} + 0.82 U_{th}^{fast\,3} - 0.28 U_{th}^{fast\,2} + 0.014 U_{th}^{fast} + 0.09$							
$rF_{pcsa}^{slow} = \begin{cases} 0, U \le U_{th}^{slow} \\ \frac{F_{pcsa}^{slow}}{1 - U_{th}^{slow}}(U - U_{th}^{slow}), U > U_{th}^{slow} \end{cases}, where \quad U_{th}^{slow} = 0.01$								
$rF_{pcsa}^{fast} = \begin{cases} 0, U \le U_{th}^{fast} \\ \frac{F_{pcsa}^{fast}}{1 - U_{th}^{fast}}(U - U_{th}^{fast}), U > U_{th}^{fast} \end{cases}, where \quad U_{th}^{fast} = F_{pcsa}^{slow} * U_r (= 0.8)$								
$W^{slow}(U, U_{th}^{fast}) = \begin{cases} W^{s1} = 1.56U^2 - 1.20U + 0.884, U_{th}^{slow} \le U < U_{th}^{fast} \\ W^{s2} = W^{s1}(U_{th}^{fast}) + A\left(1 - e^{-\frac{U - U_{th}^{fast}}{\tau_s}}\right), U > U_{th}^{fast} \end{cases}$	$A = -1.99 U_{th}^{fast\,4} + 1.90 U_{th}^{fast\,3} - 1.75 U_{th}^{fast\,2} + 1.19 U_{th}^{fast} + 0.13$							
	$\tau_s = 0.26$							
$W^{fast}(U, U_{th}^{fast}) = \begin{cases} W^{f1} = \left(\frac{U - B}{C}\right), U_{th}^{fast} \le U < U_r \\ W^{f2} = W^{f1}(U_{th}^{fast}) + D\left(1 - e^{-\frac{U - U_r}{\tau_f}}\right), U \ge U_r \end{cases}$	$B = 0.59 U_{th}^{fast} + 0.39$							
	$C = -98.82 U_{th}^{fast\,5} + 155.7 U_{th}^{fast\,4} - 85.96 U_{th}^{fast\,3} + 19.32 U_{th}^{fast\,2} - 2.62 U_{th}^{fast} + 1.02$							
	$D = 0.35$							
	$\tau_f = -0.27 U_{th}^{fast} + 0.25$							
$E_{initial}(f = f_{tet}, L_{ce} = L_{ce0}, V) = \frac{e_1 * V\hat{}2 + e_2 * V + e_3}{e_4 - V}$	e_1	e_2	e_3	e_4	e_1	e_2	e_3	e_4
	−76.6	−792	124	0.72	145	−3322	1530	1.45
Energetics constants	a				a			
	0.33				0.33			
	R				R			
	1.5				1			
	M				M			
	0.25				0.25			

Notes: Top bar $\bar{x}$ denotes the normalized variable x (forces by maximum isometric tetanic muscle force F_0, lengths and velocities by optimal fascicle length or optimal tendon length [L_{ce0} or L_{se0}]).

pended, which are the major contributors to the initial enthalpy measured. $E_{recovery}$ is therefore determined based on the initial heat rate and efficiency of the metabolic process that restores these molecules. The ratio of recovery to initial enthalpy (parameter "R" in the model) under aerobic conditions has been measured to be 1 for extensor digitorum longus (EDL; predominantly fast-twitch) and 1.5 for soleus (SOL; predominantly slow-twitch) muscles [27]. The recovery to initial enthalpy ratio has not been investigated rigorously for the anaerobic condition but it is theoretically close to that of the aerobic condition (see [27]); therefore, we chose to model the efficiency of both forms of metabolism identically. Although the dynamics of recovery are relatively slow, lasting on the order of a few minutes [30], and are impractical to study in active muscle [13], it seems sensible for the purposes of this model to represent $E_{recovery}$ as a multiple, R, of the initial heat rate (Fig. 1, STEP 6)

$$E_{recovery}(f, L_{ce}, V_{ce}) = E_{initial}(f, L_{ce}, V_{ce}) * R$$

where

$$E_{initial}(f, L_{ce}, V_{ce}) = E_{xb}(f, L_{ce}, V_{ce}) + E_a(f).$$

Note that this formulation does not capture the dynamics of the recovery rate; however, it provides a good approximation of the total recovery energy associated with particular conditions of muscle use. Also note that metabolic processes, hence R, vary across fiber types as well as with the state of muscle fatigue [15], [29]. Further experiments are needed to understand the process of fatigue before its effects on energetics and force can be modeled accurately (see Section IV-C).

4) Total Energy: The total energy rate was taken as the sum of the $E_{initial}$ and $E_{recovery}$. A conversion factor (M) obtained from [37] was then used to convert the energetic units from mW/g_{dry} to mW/g_{wet} because the wet mass is a parameter specified in VM and is more readily obtainable from the literature (Fig. 1, STEP 7)

$$E_{total}(f, L, V) = (E_{initial}(f, L, V) + E_{recovery}(f, L, V)) * M, \quad \text{in} \frac{mW}{g_{wet}}$$

C. Overall Behavior of the Model

In this section, we verify the implementation of the model and demonstrate its emergent behavior across a wide range of physiological conditions. We conclude the section with a comparison of energy and force output to show their qualitative differences and emphasize their different implications when used as teaching signals for an optimization algorithm.

1) Model Verification: The main experimental relationships on which the model is based are reproduced accurately by the model. Fig. 2 shows the $E_{initial}$-velocity relationship obtained experimentally (open squares) and that predicted by the model (solid trace) for tetanically stimulated muscle at optimal sarcomere length. The experimental and predicted relationships for both 100% slow- and 100% fast-twitch muscle agree very closely. The model's prediction is also within the experimental range of E_a (30%–40% of $E_{initial}$) obtained from [32] and [33]. Although there are some published E_a values that are significantly higher than this range, we chose not to include them as their underlying experimental techniques are questionable [32]. E_a, as computed by the model, is independent of velocity because it is assumed that myofilament motion does not affect active ion transport.

2) Effects of Fiber Composition, Excitatory Drive and Sarcomere Kinematics on Energy Consumption: Energy consumption and its partitioning have qualitative dependencies on fiber composition, excitatory drive, and sarcomere kinematics. As shown in Fig. 3, fast-twitch fibers can consume more than five times as much energy per unit time as slow-twitch fibers for the same force produced (both muscles were contracted isometrically at optimal sarcomere length).

In both slow- and fast-twitch muscle, energy consumption rises with neural drive because it increases the rate of ionic transport, hence E_a (as shown by the larger red portion of the column in Fig. 3). A rise in drive also increases the number of cross-bridges formed, leading to an increase in E_{xb} (as shown by the larger blue portion in Fig. 3). $E_{recovery}$ (marked green in Fig. 3) increases as well because it is proportional to the sum of E_a and E_{xb}.

Energy consumption also has a strong dependence on sarcomere velocity, as it increases significantly with decreasing velocity (i.e., higher rates of shortening). As velocity decreases, E_{xb} rises because cross-bridges complete their cycle at a higher rate. E_a remains the same because energy related to ionic transport is independent of velocity.

Energy consumption is reduced when sarcomere length is either shortened or stretched beyond L0. This is because in both cases there is a reduction in the number of cross-bridges formed, which reduces E_{xb}. The asymmetry mirrors the force-length relationship and is related to the different mechanisms underlying these two cases: reduced myofilament overlap in the stretched sarcomere and double myofilament overlap in the shortened sarcomere. E_a remains the same because it is independent of sarcomere length.

3) Comparison of Energy and Force Output: We computed initial energy consumption and force production for a model of human biceps longus (40% S, 60% F) as a function of fascicle velocity from -6 to $+3$ rest lengths per second (L0/s). These two results are approximately inversely related for a family of curves for neural drive in 20% steps from 0 to maximal excitation (see Fig. 4), where fiber types are recruited and frequency modulated according to the size principle [1]. Maximal force of $\sim$840 N (140% of maximal isometric force) occurs for stretching velocities greater than 1L0/s when energy consumption is $\sim$40 W. Maximal energy consumption of $\sim$330 W occurs near Vmax ($\sim -6L0/s$), when force drops to zero. Energy consumption per unit isometric force rises from 0.1 W/N at 40% drive (all slow-twitch fibers) to 0.2 W/N at 100% drive.

It is evident from Fig. 4 that force and energy measures are vastly different and they will probably lead to different neural strategies when they are incorporated into an optimization algorithm's cost function. A cost function based on muscle force (or related parameters such as torque, stress, etc.), for example,

TABLE II
SYMBOLS AND DEFINITIONS

Symbols	Definitions
U	Activation input (0-1)
F_{pcsa}^{i}	Fractional PCSA of i^{th} fiber type (0-1)
rF_{pcsa}^{i}	Recruited fractional PCSA of i^{th} fiber type (0-F_{pcsa}^{i})
U_{th}^{i}	Recruitment threshold for i^{th} fiber type (0-1)
U_r	Fractional activation level at which all fiber types for a given muscle are recruited (0-1)
U_{eff}	Effective drive, an intermediate muscle activation signal simulating calcium dynamics (0-1)
W^i	Weighting function that determines a lumped unit's (fiber type) effective Af (0-1)
F_0	Muscle maximal tetanic force (N)
L_{ce0}	Optimal fascicle length (cm)
L_{se0}	Optimal tendon length (cm)
$\bar{F}_{se}$	Series elastic element (tendon) force (F_0)
$\bar{F}_{pe1}$	Stretching contractile passive element (fascicle) force (F_0)
$\bar{F}_{pe2}$	Compressive contractile passive element (fascicle) force (F_0)
$\bar{F}_{ce}$	Active contractile element force (F_0)
$\bar{L}_{se}$	Tendon length (L_{se0})
$\bar{L}_{ce}$	Fascicle length (L_{ce0})
$\bar{L}_{ce}^{max}$	Maximum fascicle length of the muscle at its maximum anatomic musculotendon length (L_{ce0})
$\bar{V}_{ce}$	Fascicle velocity (L_{ce0}/s)
FL^i	Force-length function of i^{th} muscle fiber type
FV^i	Force-velocity function of i^{th} muscle fiber type
Af^i	Activation-frequency relationship of i^{th} fiber type
Y	Yielding factor for slow fiber type
S	Sagging factor for fast fiber type
f_{env}^{i}	Firing frequency input to 2nd order excitation dynamics of i^{th} fiber type ($f_{0.5}$)
f_{tet}	Tetanic motor unit firing rate
f_{int}^{i}	Intermediate firing frequency of 2nd order excitation dynamics of i^{th} fiber type ($f_{0.5}$)
f_{eff}^{i}	Effective firing frequency of i^{th} fiber type ($f_{0.5}$)
E_a	Energy rate related to excitation (mW)
E_{xb}	Energy rate related to crossbrige cycling (mW)
$E_{initial}$	Energy rate related to ATP and PCr consumption, E_a+ E_{xb} (mW)
$E_{recovery}$	Energy rate related to ATP and PCr recovery (mW)
E_{total}	Total energy rate per unit mass (mW/g_{wet})
a	E_a partition relative to E_{tot} for the isometric condition
R	Ratio of recovery to initial energy ($E_{recovery}$/ $E_{initial}$)
M	Muscle mass unit conversion factor (g_{dry}/g_{wet})
Act_{eff}	Effective activation of "lumped motor unit" (rF_{pcsa}^{i}*W*Af; 0-1)

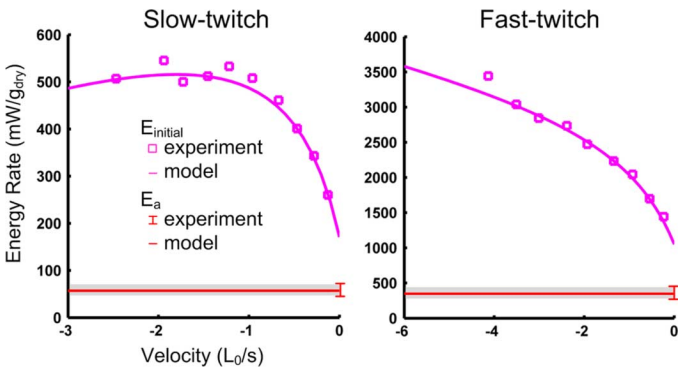

Fig. 2. Model verification. The model accurately reproduces the energy-velocity relationships presented in [15] and excitation energy as a percentage of total energy consumed presented in [32] and [33].

would lead to preferential recruitment of muscles that are shortening, whereas a cost function based on energy would lead to recruitment of muscles that are lengthening. This is particularly relevant for tasks like locomotion where subjects tend to recruit muscles during their lengthening phase to improve energetic economy of the movement (see Section IV).

III. VALIDATION

To assess the model's ability to predict energy consumption of human muscle, we validated it against data from three experiments performed *in vivo* that were independent from the datasets used to construct the model. We focused specifically on the model's ability to capture the substantial effects of fiber composition, excitatory drive, and kinematics, respectively.

A. Effects of Fiber Composition

To test the validity of the model in predicting the effects of fiber composition on energy consumption, we compared its

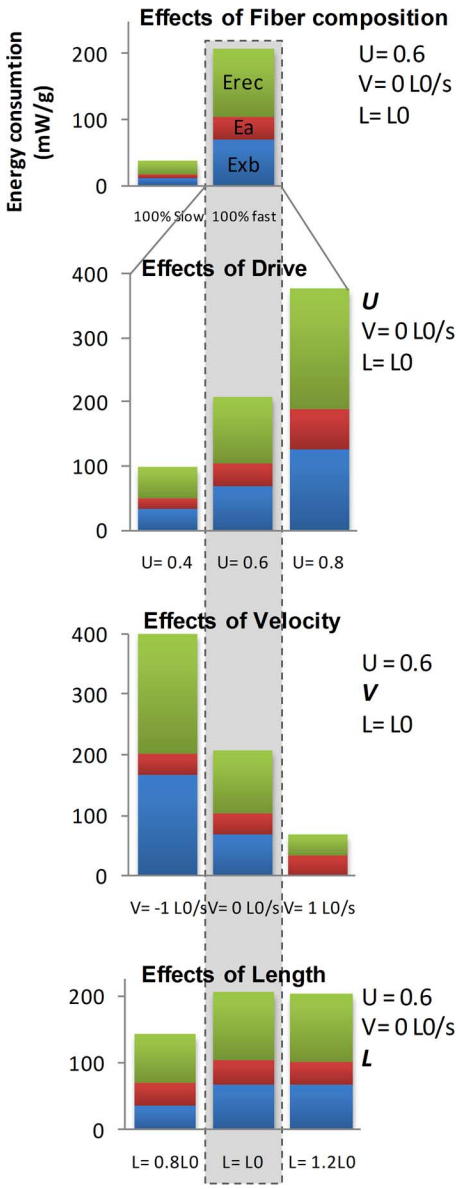

Fig. 3. Overall behavior of the model. This figure illustrates qualitative dependencies of energy consumption on fiber composition and various stimulation parameters. Stimulation parameters are shown on the right, with the varied parameter labeled in bold (U: excitatory drive; V: sarcomere velocity; L: sarcomere length). The bars within the shaded region represent energy consumption for an identical set of stimulation parameters. All bars are drawn to scale to emphasize the relative effects on energy consumption resulting from different stimulation conditions. Energy is partitioned according to the major physiological processes that underlie it to illustrate the dependency of each process on the varied parameter.

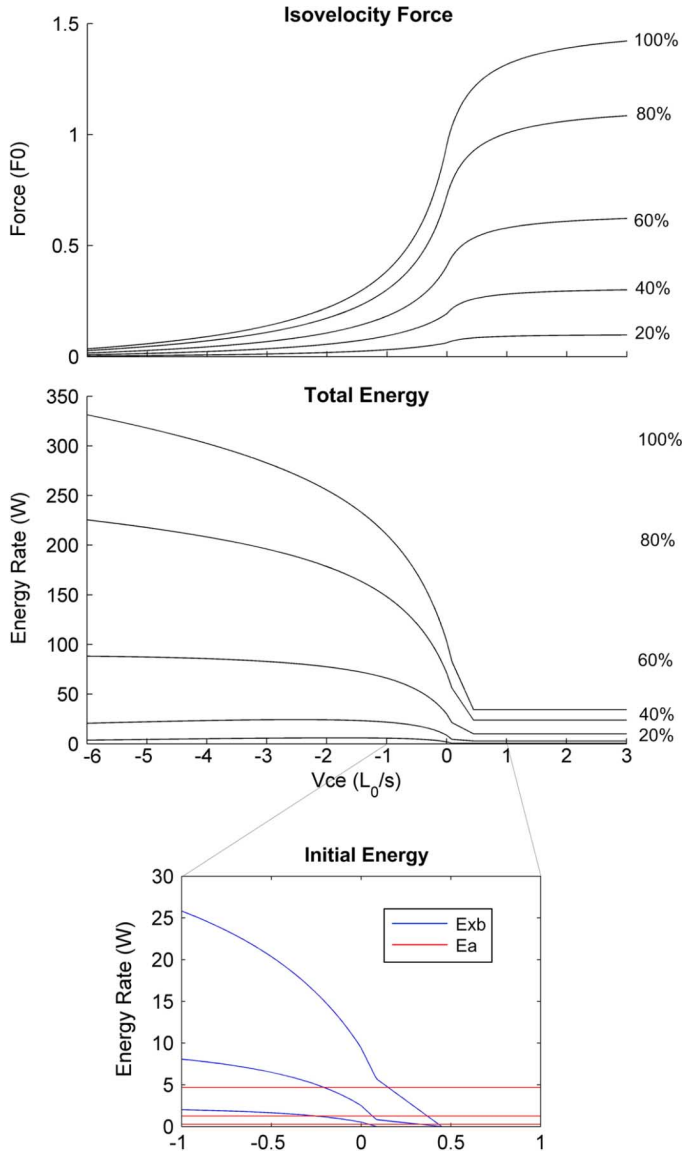

Fig. 4. Comparison of force production (top) and total energy rate (middle) under identical conditions of stimulation. Energy and force-velocity relationships are shown for a representative muscle analogous to the long head of the biceps (40% slow/60% fast-twitch fibers; $\mathrm{mass} = 300$ g; $\mathrm{F0} = 600$ N; $\mathrm{L0} = 16$ cm). Velocities ranged between $-6\mathrm{L}_0$/s and $3\mathrm{L}_0$/s and excitatory drive ranged from 20% to 100% as shown next to the plots on the right. Lower graph shows initial energy rate (partitioned into $\mathrm{E_{xb}}$ and $\mathrm{E_a}$) for $\pm 1\mathrm{L}_0$/s and midrange excitatory drives ($\mathrm{U} = 20\%, 40\%$, and 60%MVC), which reflect common conditions of use.

output to the results from [38]. In this experiment, the temperature rate was measured at MVC for a variety of human muscles (soleus, sacrospinalis, biceps brachii) that covered a wide range of fiber compositions ($\sim$0%–70% fast-twitch fibers). To make a fair comparison between the model and experimental data, we considered that although the subjects were instructed to contract their muscles maximally, they tend not to reach true MVC without intensive training [39]. Reference [38] did not mention such training nor did it employ the twitch interpolation technique of [39] to confirm MVC. The increase in force generated by the stimulation would have indicated how close to maximal the muscle was actually firing, helping identify the true MVC value.

Experimental results and model predictions for two cases are shown in Fig. 5. The predicted energy rate is shown for the cases where the subjects attained true MVC (experimental MVC corresponds to $\mathrm{U} = 1$) and an underestimated MVC (experimental MVC corresponds to $\mathrm{U} = 0.8$). Both cases reproduce the strong positive correlation between percentage of fast-twitch fibers and energy consumption, with the second case $(\mathrm{U} = 0.8)$ being in close agreement with the data in terms of absolute value and slope.

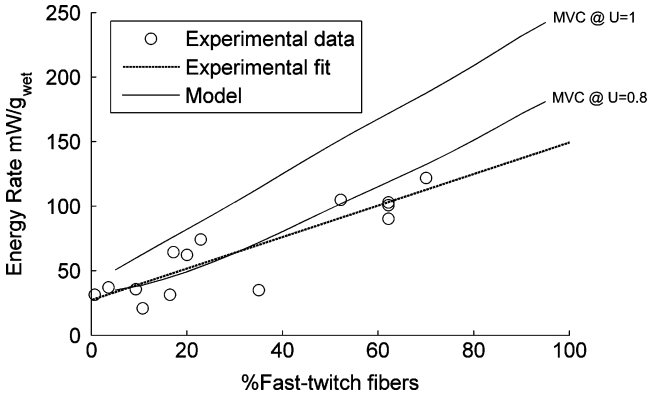

Fig. 5. Validation results for effects of fiber composition. Experimental results and model predictions are plotted for the rate of energy consumption as a function of fiber composition. Muscles were assumed to be contracted isometrically at their optimal length. Fiber composition is labeled on the abscissa as the percentage of fast-twitch fibers present in the muscle. The two traces are shown as model predictions that correspond to scenarios in which subjects achieved maximal drive (MVC @ $\mathrm{U} = 1$) and undershot it by 20% drive (MVC @ $\mathrm{U} = 0.8$), respectively.

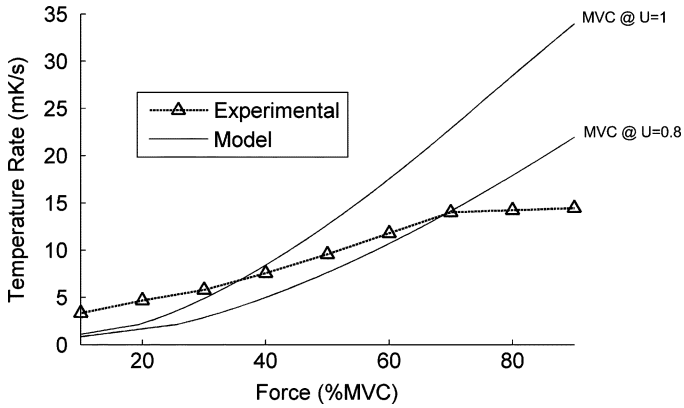

Fig. 6. Validation results for effects of excitatory drive. Experimental results and model predictions are plotted for muscle temperature rate as a function of isometric force. Muscles were assumed to be contracting isometrically at their optimal length. Force on the abscissa is normalized by the force produced at maximal effort. Two traces are shown for model predictions that assume the human subjects truly achieved maximal drive (MVC @ $\mathrm{U} = 1$) and undershot it by 20% (MVC @ $\mathrm{U} = 0.8$). It was assumed that the vastus lateralis muscle in this study was composed of approximately equal portions of slow and fast-twitch fibers.

B. Effects of Excitatory Drive

To assess the model's performance for submaximal contractions, we compared its predictions to results from Saugen and Vollestad [40]. Temperature rate of the vastus lateralis muscle was measured during isometric contractions for forces ranging from 10% to 90% MVC. Assuming that the thermocouple measurements represented the average temperature of the muscle and a negligible amount of heat escaped the muscle, the rate of heat production would be related simply to temperature rate through the heat capacity of muscle. Thus, to compare our model's predictions to the temperature measurements, we converted energy consumption (which is equivalent to heat liberation in this case) to temperature rate by dividing it by the heat capacity of muscle (3.75 kJ/kg; [40]).

As in the previous section, we considered that the subjects in this experiment may have not reached true MVC. Experimental results and model predictions for the cases where true MVC was attained or underestimated are shown in Fig. 6. If we make the reasonable assumption that subjects undershot the true maximal drive by 20% we get a substantially better agreement in terms of the absolute value and qualitative relationship between temperature rate and excitatory drive. Nevertheless, there is some deviation between the model output and experimental results. The model probably underestimates energy consumption at low force levels because it does not fully take into account the squirming motion (see Section II-A) of the myofilaments, which may be more pronounced at these levels because of the nonlinear compliance of biological connective tissue at low stresses. As force increases the squirming motion reduces and the deviation expectedly decreases. Furthermore, their measured heat values include some recovery energy because of the duration of the contractions, which were much longer for the low contractile force (15 s for 10%MVC to 6 s for 90%MVC). This would also overestimate initial energy consumption at low forces more than at high forces, flattening the experimental relationship. The plateau of the experimental data above 70%MVC may relate to increasing heat loss into adjacent, cooler tissues.

C. Effects of Kinematics

In order to validate the effects of kinematics on energy consumption, we compared our model's prediction to observations from [41]. Their experiment followed the dynamic knee extension paradigm [42] in which subjects are hooked up to a cycle ergometer and trained to extend their knee from a neutral sitting posture ($\sim$80 degrees extension) to nearly full extension and passively return to the neutral posture. The task is designed to recruit only the quadriceps muscles, which are active mostly in the first phase of the extension when the shank and foot are accelerating. Subjects in this study were asked to perform the task with maximal effort (i.e., as fast as possible) for three minutes while the rate of metabolic energy consumption (heat production plus mechanical power output) was estimated.

Initially, we anticipated that actual rate of energy consumption would differ significantly from our model's prediction. Energy rate in the experiment increased by approximately 40% from the beginning to the end of each session whereas our model's prediction would stay constant because it is solely dependent on muscle recruitment level and kinematics, which are virtually the same across extension cycles. We hypothesized that the observed increase in energy rate was due to the dynamics of the ATP/PCr recovery process, which has a relatively long time constant. While the energy consumed by the recovery process is captured by the model presented here, its dynamics are not (see Section II-B3). To estimate these dynamics we used the energy rate response during the recovery phase of a brief contraction [27] as the impulse response characterizing the ATP/PCr recovery system. See Appendix B for details on how the task and associated energy consumption were modeled.

As shown in Fig. 7, the model's prediction matches experimental results very closely, given the reasonable assumption that subjects' effort was not truly maximal (see Sections III-A and III-B). The model captures the dynamics of energy consumption and the total amount consumed (model: 35 000 J; experiment: 30 000–40 000 J; integral of curves in Fig. 7) remarkably well.

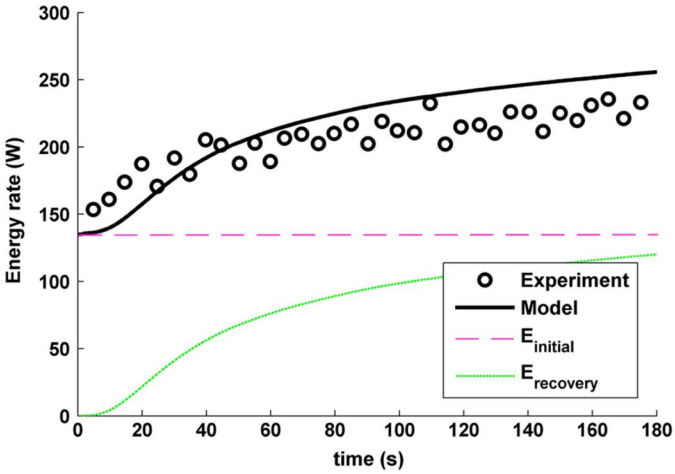

Fig. 7. Validation results for effects of kinematics. Experimental results and model predictions are shown for the dynamic knee extension task (see text for details) performed over three minutes. Both $\mathrm{E_{initial}}$ and $\mathrm{E_{recovery}}$ contribute significantly to the total energy rate due to the long duration of the task. As in the experiment, the energy rate computed by the model was averaged over one second intervals (equivalent to one cycle of the movement). $\mathrm{E_{initial}}$ is constant throughout the entire duration of the task because the stimulation parameters are constant but $\mathrm{E_{recovery}}$ increases over time due to the dynamics of metabolism (see Appendix B for details).

For the brief contractions studied by [27], the recovery process produces little or no lactate, hence relies on oxidative metabolism, which takes longer to complete and actually generates more heat per unit ATP regenerated. Thus, the time constant and scaling factor for fast-twitch fibers derived from this experiment applies to the first couple of cycles of the cycle ergometry, but quickly shifts to a shorter time constant and lower scaling factor as the recovery process shifts toward anaerobic metabolism. The model results in Fig. 7 do not incorporate such a shift, whose dynamics are not known, but either change would tend to improve the agreement between experiment and model.

IV. Discussion

A. Limitations

The lumped model described here is currently limited to two fibers types, which we have identified as fast- and slow-twitch; a more general version of the VM modeling software does support arbitrary numbers of motor units and fiber types [1]. In reality, many muscles are composed of a range of fiber types whose force-generating and metabolic properties reflect different mixtures of those that we have associated with our fast- and slow-twitch models [43]. Fast-twitch fibers are often divided into type IIb (type IIx in humans), which typically utilize glycolytic metabolism, and type IIa, which typically utilize oxidative metabolism, similarly to slow-twitch fibers. The energetics model is based primarily on experiments performed on mouse soleus (SOL) and extensor digitorum longus (EDL) muscles, which are composed mostly of type I and type IIa fibers, respectively [44]. In a muscle with a large proportion of type IIb/x fibers, our estimate of recovery energy will likely be too high, as glyocolytic pathways are known to produce less heat per ATP regenerated; the theoretical ratio of recovery to initial energy for glycolytic metabolism is 0.8 whereas that of oxidative metabolism is 1.13 [27], [45]. It is important to note that these estimates depend on the energy source (e.g., carbohydrate versus fat) and other conditions in the sarcoplasm (e.g., ionic and metabolite concentration). Furthermore, the theoretical estimate for glycolysis does not include the energy cost associated with the extra step of handling the lactate byproduct (e.g., converting it to pyruvate for later use in oxidative pathways). More rigorous experimentation and analysis of metabolic efficiency are necessary to assess their actual contribution to muscle energetics.

The model should be used with care when simulating tasks in which the muscles involved may experience fatigue because the effects of fatigue on force production and energy consumption are not included in our model. Fatigue, for example, has been associated with significant changes to the energy and force-velocity relationships [15]. We chose not to incorporate these effects into the model because they are specific to a particular state of fatigue, which may consist of a mixture of several mechanisms that are too poorly understood to model individually. The ratio of recovery to initial heat also varies with the degree of fatigue in fast-twitch EDL muscle [29], which is also not included in the model.

The ratio of activation energy to total energy, constant term "a" in our model, may have some dependence on firing rate. There are numerous competing effects on "a" from phenomena that are dependent on firing rate such as calcium release efficiency, mechanical squirm (related to the noise in force output and muscle stiffness) and cross-bridge cooperativity. Unfused contractions elicited by submaximal firing rates, for example, cause larger oscillations in output force and sarcomere length than in the tetanic condition. These oscillations should produce a higher cross-bridge cycling rate than would be expected if the contraction were completely fused as in the tetanic condition and therefore may reduce "a". The dependence of "a" on firing rate has not yet been investigated systematically but it is likely that it is a small effect based on the finding that the ratio was nearly the same for a submaximal and tetanic frequency of stimulation in fast-twitch muscle [33]. This is somewhat counter-intuitive, because $\mathrm{E_a}$ might be expected to continue to rise with firing rate even as output force plateaus. It may be that the calcium reservoir in the cisternae starts to deplete at approximately the same time as the sarcoplasmic calcium concentration reaches saturation for troponin binding, reflecting efficient design. Nevertheless, if a salient dependency emerges from new data, the model is sufficiently modular so that the "a" term can be readily modified to account for it.

"Motor noise" (fluctuating recruitment of individual motoneurons; [46]) produces force fluctuations that act against the series-elasticity of tendons and aponeuroses to produce fluctuations in fascicle and sarcomere length that should increase cross-bridge cycling for a given nominal velocity of the muscle-tendon unit. VM includes an explicit model of the series-elasticity and the lumped recruitment model is designed to generate force fluctuations reflecting whatever model of motor noise is added into the driving excitation signal [34]. Therefore, energy consumption associated with motor noise

should be correctly incorporated into the predictions of this new version of VM.

B. Role in Motor Control Research

Even with an accurate energetics model at hand, using it to gain insight into the neural strategies underlying motor tasks remains a challenge. Although the nervous system appears to consider metabolic energy consumption when selecting movement strategies, it does not always pick the most energy efficient strategies. For example, energetics are obviously less important if the task is to reach to a target 10 times versus 1000 times. Furthermore, if subjects expect a perturbation while performing a task, they are likely to cocontract more during the movement to resist it, which could be mediated through a reduced emphasis on energetics. There is also evidence that energetic considerations change as subjects learn to perform a task, starting with excessive cocontraction initially and gradually reducing it as they learn to use more efficient feedforward and feedback strategies to improve their kinematic performance [8], [9]. Tsianos *et al.* [47] studied motor learning in a planar arm model, which was much more reliable when the system started with cocontraction and then learned to perform well without it. Such high level strategizing can be expected to emerge from motor learning when the cost function includes realistic changes over time in the relative importance of kinematics and energetics.

The fact that force output and energy consumption actually move in opposite directions around zero velocity may shed light on speculations about the role of biarticular muscles [48]–[55]. Biarticular muscles tend to be active when the two joints that they cross are moving in opposite directions. The net muscle velocity tends to be close to zero or to reverse sign while these muscles are active, making them specifically well-suited for economical transfer of momentum from segment to segment, avoiding the need to dissipate excessive kinetic energy as heat.

The optimization techniques described in the Introduction all require minimization of a cost function to predict the roles of individual muscles for a given task. When such cost functions are applied to engineering problems, they usually consist of a combination of terms related to speed, accuracy and energetic cost. The model provided here permits the development of analogous cost functions for biological systems rather than the arbitrary minimization of total force or recruitment that is generally used instead.

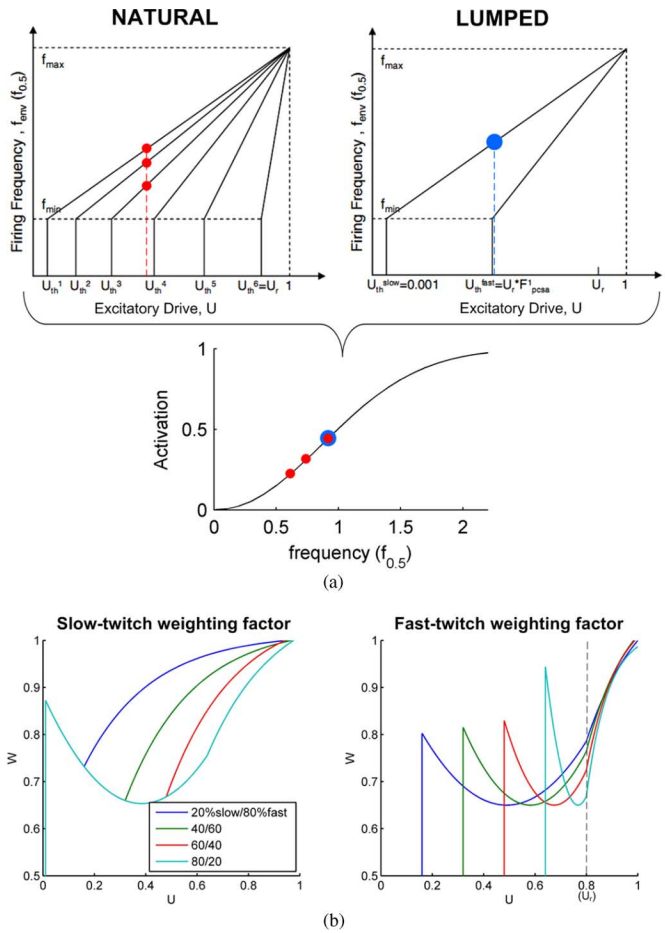

Fig. 8. Comparison of "Natural" and "Lumped" recruitment schemes (a). Motor units in the "Natural Units" scheme are recruited sequentially according to fiber type and size. In "Lumped" recruitment, each fiber type is represented by a single motor unit whose frequency modulation is identical to the first recruited unit within the corresponding fiber type in the "Natural Units" scheme. The plot at the bottom illustrates the error resulting in activation (which scales force and energy) given this approximation and highlights the need of a weighting function to capture the nonlinear effects on activation caused by sequential recruitment of discrete motor units. Weighting functions for slow and fast-twitch fibers (b). A weighting function is shown for each fiber type that matches the steady state force computed by the "Lumped" model to that of "Natural Units." The weighting function is dependent on excitatory drive as well as fiber composition. Vertical lines mark the recruitment threshold of the fiber type. See text and Tables I and II for a detailed description of the functions that generate these curves.

C. Role in Studying Effort and Fatigue

VM with energetics can also be used as a tool to understand and model fatigue. Fatigue is a collection of incompletely understood phenomena in which motor units change their properties as a result of excessive muscle use and/or insufficient oxygen supply to the muscle fibers, depending on factors such as metabolic demand of the task, stored energy reserves, and hydrostatic pressure and capillary bed structure. It is associated with reduced force production and slower dynamics, at least in part from reduced availability of ATP for processes related to both activation and cross-bridge cycling [29], [56], [57]. The effects, however, are only qualitatively understood, hence the vague categorization of fatigue into moderate and excessive. The effects also interact with other time-varying processes such as potentiation, both of which are particularly prominent in fast-twitch muscle [58]. Because the terms of the functions in VM correspond to identifiable physiological processes, it should be relatively straightforward to modify their coefficients to reflect the various effects observed in association with fatigue [56], but this remains to be done.

Understanding the process of onset and reversal of fatigue during physiological conditions would benefit greatly from the model presented here because the energetic cost is a measure of metabolic demand, and therefore can help estimate when it would exceed chemical supplies of stored energy. The division of muscle models into slow and fast fiber types is important because they have substantially different energy rates, energy stores, metabolic processes and fatigue mechanisms. These differences have significant effects on the magnitude and nature of

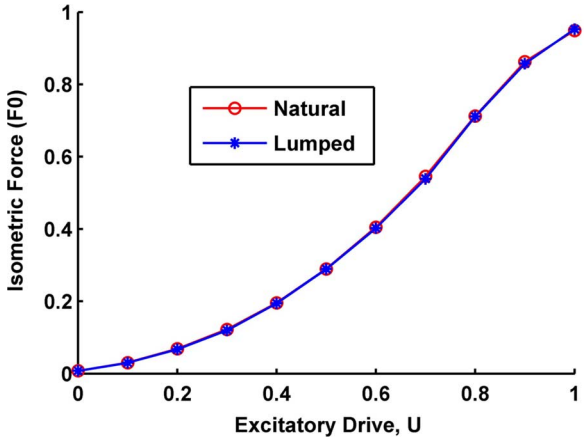

Fig. 9. Comparison of steady state response to an excitatory step. The force predicted by "Natural" and "Lumped" recruitment schemes is shown for excitatory drives ranging from 0 to 1 (maximum). The predictions of the two schemes are nearly identical.

fatigue phenomena because they affect the rate at which stored fuel is consumed.

Adaptive controllers that learn to minimize a cost-function require "knowledge of results" as a teacher, so it will be important to extend this model of energy consumption by muscle to predict metabolic products and other effects that can be sensed by the nervous system. Aerobic and anaerobic metabolism of slow- and fast-twitch muscles, respectively, have substantially different effects on CO_2 production, oxygen consumption, lactic acid excretion and heating. Neural sensors related to energy consumption presumably include intramuscular chemoreceptors for pH and oxygen, efference copy from the motoneurons, afferent, and efferent-copy signals related to increased respiratory effort, and other manifestations of increased heat dissipation such as body temperature and perspiration. While there is substantial evidence that subjects perceive and attempt to minimize energy consumption and fatigue when performing repetitive tasks, there is also paradoxical evidence that they do not compensate for fatigue once it has occurred [59]. The fiber-type specific model of energy consumption presented here provides a starting point for a quantitative model of the many perceived and silent consequences of muscle work.

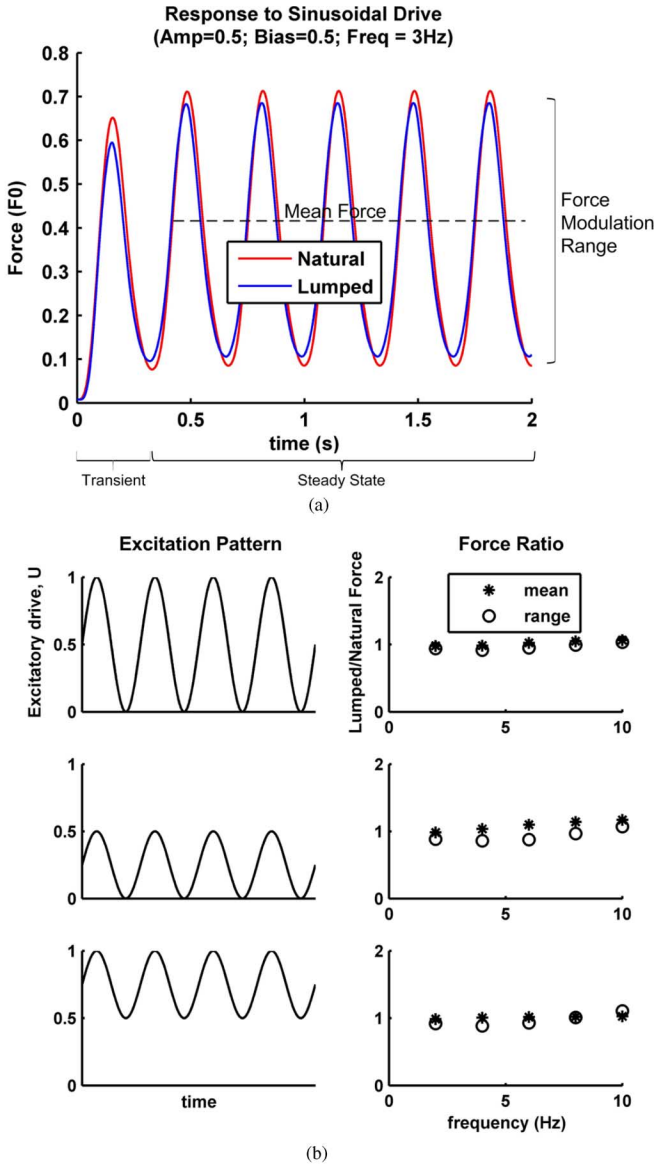

Fig. 10. Comparison of dynamic response to sinusoidal input. Predictions of "Natural" and "Lumped" recruitment schemes are shown for an exemplary stimulus (a). The response is divided into a transient and steady state phase, which is divided further into mean force and modulation range components. A comparison of these components across a wide range of amplitudes and excitation frequencies is shown in (b).

Appendix A
Virtual Muscle "Lumped Units" Algorithm

We have modified the VM continuous recruitment algorithm [34] to have sufficient modularity for the formulation of energetics and to improve accuracy in force and energy estimates without compromising its computational efficiency. The new recruitment algorithm presented here is termed "Lumped Units." The original VM ("Natural Units" [1]) divided the muscle into discrete motor units, each of which could be recruited and frequency modulated according to Henneman's size principle. While various exceptions to this stereotyped recruitment have been reported, it accounts well for motoneuron activity reported under dynamic locomotor conditions [60] similar to those obtaining in the cycle ergometry task [41] used for validation-effects of kinematics (Section III-C). Obtaining a smoothly modulated total muscle force required a model with many summed units, which was computationally too expensive for multimuscle systems. Song *et al.* [34] provided a lumped recruitment algorithm that allowed each muscle fiber type to be represented by a single motor unit with a smoothly modulated firing rate and a gradually increasing percentage of the PCSA representing its share of the total muscle. This reduces the number of states to be solved (from $2+3*\#$ of motor units to $3+3*\#$ of fiber types). Retaining force-length, activation, and recruited fractional physiological cross-sectional area (fPCSA) terms from the natural recruitment algorithm allow independent calculation of energy consumption for slow and fast fibers and to scale the tetanic enthalpy data. We here introduce a weighting

function that computes an effective activation for each fiber type that more accurately reflects the sum of the nonlinear relationships relating excitation to firing rate of each motor unit. Because sarcomeres move almost homogeneously during muscle contraction and their individual contributions to total muscle force sum approximately linearly, the force-length and force-velocity relationships have identical form in the lumped model. The recruited fractional physiological cross sectional area $(\mathrm{rF_{pcsa}})$ term for each fiber type is also preserved in the lumped model, as it is important for scaling the energy consumption of each fiber type. The modifications and additions presented here do not add significantly to the computational load, so the reductions in computing time reported by [34] for lumped recruitment still obtain for this new version of VM.

Motor units are recruited continuously in this scheme; therefore, we modeled $\mathrm{rF_{pcsa}}$ for a given fiber type as a linear function of drive that is zero when the drive is equal to threshold and equal to its $\mathrm{F_{pcsa}}$ at maximal drive

$$rF^i_{\mathrm{pcsa}} = \begin{cases} 0, & U \le U^i_{\mathrm{th}} \\ \frac{F^i_{\mathrm{pcsa}}}{1-U^i_{\mathrm{th}}}\left(U - U^i_{\mathrm{th}}\right), & U > U^i_{\mathrm{th}} \end{cases}$$
$$\text{where} \quad \mathrm{i} = \mathrm{slow}, \mathrm{fast}.$$

We chose a weighting function that modulates the activation of the lumped units such that the steady state force matches that of the discrete model. For an arbitrary drive between 0 and maximal (normalized to 1) the activation of the lumped unit overestimates the total activation of the discrete motor units because the later recruited units within that fiber-type will be firing at lower rates than the first recruited unit [see Fig. 8(a)]. To compensate for this discrepancy across different fiber compositions (represented by parameter $U^{\mathrm{fast}}_{\mathrm{th}}$) and neural drive (U), we created the weighting function shown in Fig. 8(b). It is a two-part piece-wise function in which the first part is a parabola spanning from the fiber type's stimulation threshold to the threshold of the next recruited fiber type for the slow fiber type and $\mathrm{U_r}$ for the fast fiber type. The second part is an exponential that is defined all the way to maximal drive, shown in the equation at the bottom of the page.

The resulting steady state force prediction ($rF_{\mathrm{pcsa}} * W * Af * FL * FV$) of the new algorithm is nearly identical to that of the "Natural Units" model (see Fig. 9). To match the dynamic response, we subjected the input drive to a first-order low pass filter with a variable time constant depending on whether the drive is increasing or decreasing. Without this filter the weighting function and consequently the muscle force at an intermediate activation would change instantaneously in response to a drive, which is unphysiological. To model the complex dynamics resulting from newly recruited units that are not captured by the lumped unit, we made the time constant for rising drive a function of the change in drive $(\mathrm{U} - \mathrm{U_{eff}})$. The exact form of the function varies with fiber type composition because fiber types have rise and fall times that differ significantly. For decreasing drive, a simple time-constant irrespective of drive was sufficient

$$\dot{U}_{\mathrm{eff}} = \frac{U - U_{\mathrm{eff}}}{T_U}$$
$$T_U = \begin{cases} T_{\mathrm{rise}} e^{-(U-U_{\mathrm{eff}})*\ln(T_{\mathrm{rise}}*1000)}, & U \ge U_{\mathrm{eff}} \\ T_{\mathrm{fall}}, & U < U_{\mathrm{eff}} \end{cases}$$

where

$$T_{\mathrm{rise}} = 0.38{U^{\mathrm{fast}}_{\mathrm{th}}}^2 + 0.8U^{\mathrm{fast}}_{\mathrm{th}} + 0.14$$
$$T_{\mathrm{fall}} = -0.32{U^{\mathrm{fast}}_{\mathrm{th}}}^4 + 0.82 * {U^{\mathrm{fast}}_{\mathrm{th}}}^3 - 0.28{U^{\mathrm{fast}}_{\mathrm{th}}}^2 + 0.014U^{\mathrm{fast}}_{\mathrm{th}} + 0.09$$

Fig. 10 shows a comparison of the dynamic force response between "Natural" and "Lumped" algorithms for a wide range of stimulation frequencies and amplitudes. Fig. 10(a) shows the similarity in both the transient and steady state response, which can be decomposed into mean force and modulation range as shown in Fig. 10(b).

$$W^{\mathrm{slow}}(U, U^{\mathrm{fast}}_{\mathrm{th}}) = \begin{cases} W^{s1} = 1.556U^2 - 1.203U + 0.8844, & U^{\mathrm{slow}}_{\mathrm{th}} \le U < U^{\mathrm{fast}}_{\mathrm{th}} \\ W^{s2} = W^{s1}\left(U^{\mathrm{fast}}_{\mathrm{th}}\right) + A * \left(1 - e^{-\frac{U - U^{\mathrm{fast}}_{\mathrm{th}}}{\tau_s}}\right), & U > U^{\mathrm{fast}}_{\mathrm{th}} \end{cases}$$

where

$$A = -1.99{U^{\mathrm{fast}}_{\mathrm{th}}}^4 + 1.899{U^{\mathrm{fast}}_{\mathrm{th}}}^3 - 1.748{U^{\mathrm{fast}}_{\mathrm{th}}}^2 + 1.186U^{\mathrm{fast}}_{\mathrm{th}} + 0.1298$$
$$\tau_s = 0.261$$
$$W^{\mathrm{fast}}(U,\, U^{\mathrm{fast}}_{\mathrm{th}}) = \begin{cases} W^{f1} = \left(\frac{U-B}{C}\right)^2 + \ 0.65, & U^{\mathrm{fast}}_{\mathrm{th}} \le U < U_r \\ W^{f2} = W^{f1}(U_r) + \ D * \left(1 - e^{-\frac{U - U_r}{\tau_f}}\right), & U \ge U_r \end{cases}$$

where

$$B = 0.5859U^{\mathrm{fast}}_{\mathrm{th}} + 0.3934$$
$$C = -98.82{U^{\mathrm{fast}}_{\mathrm{th}}}^5 + 155.7{U^{\mathrm{fast}}_{\mathrm{th}}}^4 - 85.96{U^{\mathrm{fast}}_{\mathrm{th}}}^3 + 19.32{U^{\mathrm{fast}}_{\mathrm{th}}}^2 - 2.618U^{\mathrm{fast}}_{\mathrm{th}} + 1.023$$
$$D = 0.35$$
$$\tau_f = -0.268U^{\mathrm{fast}}_{\mathrm{th}} + 0.2548.$$

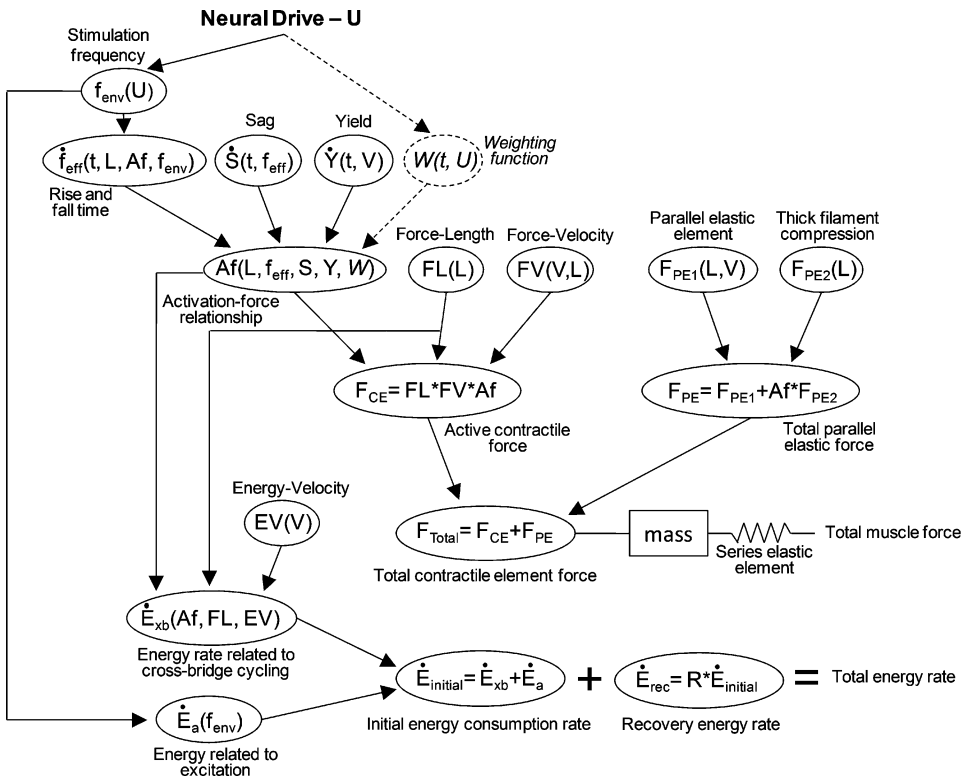

Fig. 11. Conceptual overview of functions that comprise the force and energetics models as well as their interactions. Most of the functions have a one-to-one correspondence with physiological processes underlying experimental phenomena from which the data were obtained. See text for details.

A conceptual overview of VM's force and energetics models is shown in Fig. 11. Equations corresponding to each term are provided in Table I and symbols are defined in Table II. The contractile force and energy consumption of muscle can be separated into contributions from a number of physiological processes, some of which affect both formulations. The force produced by the contractile element strains the series elastic element (representing the tendon/aponeurosis) through an intermediate mass to generate a pulling force on the attached segments. The contractile force has passive and active contributions. The passive portion is a result of the visco-elastic properties of stretching muscle and the elastic properties of the thick filament upon compression at short muscle lengths. The active portion can be divided into three major physiological processes: activation-force (Af), force-length (FL), and force-velocity (FV). The FV relationship is mainly related to the overall strain of cross-bridges, which depends on the angle of attachment of the myosin heads onto the actin sites. The FL relationship captures the effect of myofilament overlap on force and is related to the number of cross-bridges formed. The Af relationship reflects the portion of overlapping myofilaments that bind and is dependent on firing rate, muscle length and fiber-specific properties (e.g., sag and yield). The weighting function, W, only applies to the lumped recruitment model and is used to scale the activation-force relationship of the lumped unit in order to match the total Af of a realistic ensemble of motor units. The effective frequency input $(\mathrm{f_{eff}})$ to the Af relationship is determined by calculating the stimulation frequency $(\mathrm{f_{env}})$ first, which is directly proportional to the neural drive (U) if U is greater than the firing threshold. A second-order low pass filter, whose exact form depends on fascicle length and activation, is then applied to $\mathrm{f_{env}}$ to obtain $\mathrm{f_{eff}}$. Because Af and FL together provide a measure of the number of cross-bridges, they also affect the energy related to cross-bridge cycling $(\mathrm{E_{xb}})$. They are used to scale the tetanic EV relationship obtained experimentally at optimal sarcomere length. The energy related to excitation $(\mathrm{E_a})$ is simply a function of stimulation frequency, which is added to $\mathrm{E_{xb}}$ to obtain the total energy rate during the initial phase of contraction $(\mathrm{E_{initial}})$. This energy represents the amount of ATP and PCr molecules consumed and therefore determines the energy needed to resynthesize them $(\mathrm{E_{recovery}})$. The sum of $\mathrm{E_{initial}}$ and $\mathrm{E_{recovery}}$ is the total energy rate.

Appendix B
Modeling Details for Dynamic Knee Extension Task

To compute metabolic energy consumption associated with the dynamic knee extension task, we built a model that mimicked basic biomechanical properties of the leg and the performance conditions of the experiment. Because the task lasted for a relatively long period of time, it was important to include the dynamics of energy consumption related to recovery in the energetics formulation (see Section III-C).

Musculoskeletal System

The musculoskeletal model of the leg consisted of two segments (thigh and shank plus foot) linked by a hinge joint at the knee. Two muscle elements were included to represent the knee extensors, the only active muscles in this task. One element

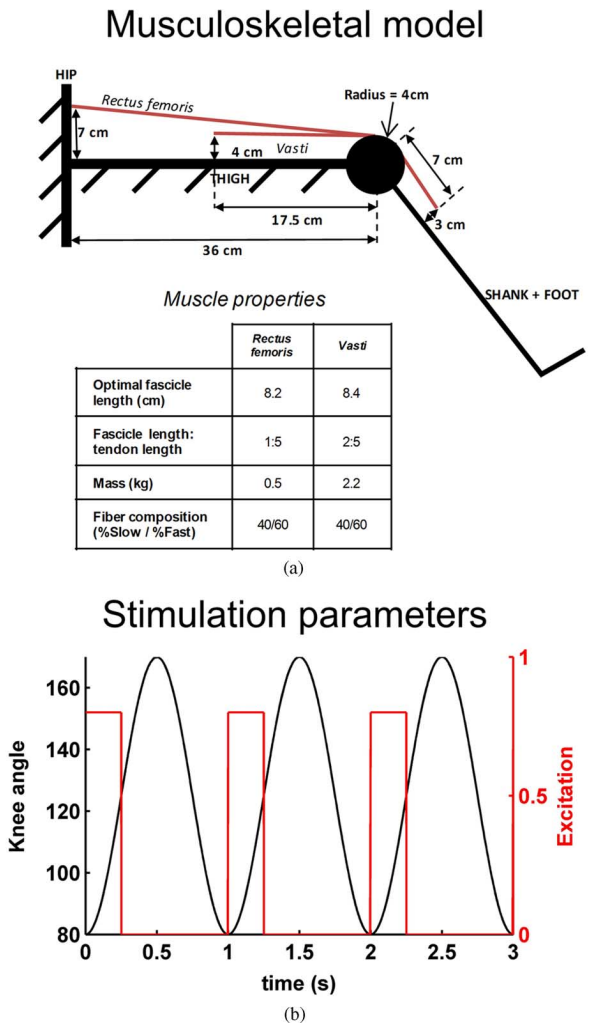

	Rectus femoris	Vasti
Optimal fascicle length (cm)	8.2	8.4
Fascicle length: tendon length	1:5	2:5
Mass (kg)	0.5	2.2
Fiber composition (%Slow / %Fast)	40/60	40/60

(a)

(b)

Fig. 12. Musculoskeletal model of the knee (a). Two separate VM elements are included representing the rectus femoris and vasti muscles, whose properties are listed in the table. Stimulation parameters (b). The knee was constrained to follow a sinusoidal trajectory ranging from 80° to 170° of extension. Both muscles were excited at 80% of their maximal drive during the first quarter of each movement cycle (acceleration phase). Stimulation parameters are shown for the first three seconds of the simulation to illustrate their relative phasing. The actual duration of the exercise was 180 s.

corresponded to the rectus femoris muscle and the other to the vasti muscles (vastus lateralis, intermedius, and medialis). The vasti muscles were lumped together because they have similar attachment points, moment arms and excitatory drive for this specific task. Rectus femoris was modeled separately because it has a longer tendon, whose compliance would affect fascicle velocity during this dynamic task. It can be assumed that they are all recruited to similar levels because the modeled task required subjects to use maximal effort. The dimensions of the skeletal segments and muscle attachment points were derived from [61]. All muscles attach to the same point on the shank via the patella, thus they have the same moment arm, which is virtually independent of joint angle [62]. Morphometric measures of the muscles such as fascicle to tendon length ratios were obtained from [63] and the shape of the maximal isometric torque versus joint angle was validated against human data presented in [64]. Muscle mass was derived from data presented in [41], [63].

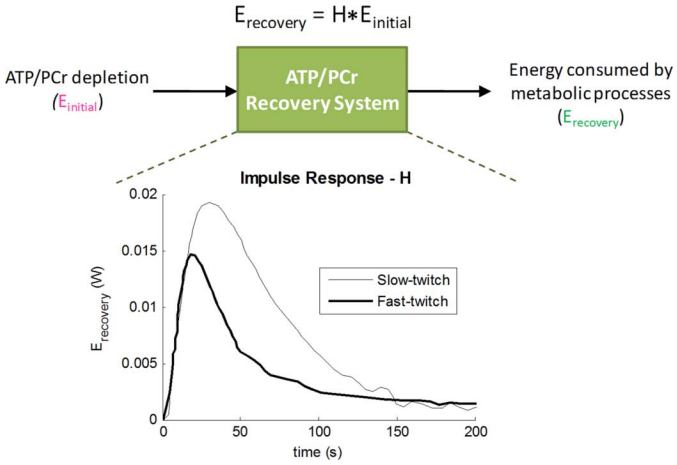

Fig. 13. Characterization of the ATP/PCr recovery system. The system accepts the rate of energy consumed due to ATP/PCr turnover ($\mathrm{E_{initial}}$) as an input and generates the energy rate corresponding to the metabolic processes needed to replenish the expended ATP/PCr. The traces displayed on the bottom of the figure were digitized and rescaled from Leijendekker and Elzinga [27], who measured $\mathrm{E_{recovery}}$ following brief tetanic stimuli. These signals were convolved with $\mathrm{E_{initial}}$ to determine the dynamics of $\mathrm{E_{recovery}}$. See text for details.

See Fig. 12(a) for a detailed description of the musculoskeletal system.

Stimulation Parameters

Stimulation parameters were chosen to model muscle excitation and kinematic conditions of the experiment in [41]. The movement performed by the subjects was smooth and periodic, so it was modeled as a sinusoidal trajectory. This kind of maximal performance generally requires "bang-bang" controls in which all and only those muscles that can contribute positive work at a given phase of the task are maximally recruited [65]. Therefore we activated both modeled muscles at 80%MVC (see Section III-A) during the first quarter of the movement cycle, which corresponded to the acceleration phase of the knee extension movement. Refer to Fig. 12(b) for a graphical depiction of the stimulation parameters.

Dynamics of Recovery Energy

As mentioned in Section II-A, every ATP and PCr molecule expended must be replenished via metabolic processes. These metabolic processes consume energy ($\mathrm{E_{recovery}}$) and last on the order of a few minutes. The hydrolysis of ATP and PCr molecules is closely related to the $\mathrm{E_{initial}}$ term in the model and can therefore be used to drive the formulation of $\mathrm{E_{recovery}}$. The formulation used for this task is based on the assumption that the recovery system behaves linearly for the range of ATP and PCr deficits occurring in the subjects' muscles. This allows complete characterization of the system's behavior based on its impulse response, which is derived for slow and fast-twitch fiber types from [27] during brief tetanic contractions that activate only aerobic metabolism in both fiber types (see Section III-C). Because the duration of $\mathrm{E_{initial}}$ measured in this experiment was small compared to the duration of $\mathrm{E_{recovery}}$, it was assumed that the $\mathrm{E_{recovery}}$ reported was the response to an impulse weighted by the total energy consumed in phase with the contraction. Therefore, the unit impulse response incorporated

into the model (shown in Fig. 13) is the measured trajectory of $E_{recovery}$ divided by the total energy consumed during the contraction.

ACKNOWLEDGMENT

The authors would like to thank N. Li for technical assistance with implementing the model in software.

REFERENCES

[1] E. Cheng, I. E. Brown, and G. E. Loeb, "Virtual muscle: A computational approach to understanding the effects of muscle properties on motor control," *J. Neurosci. Methods*, vol. 101, pp. 117–130, 2000.

[2] A. Pedotti, V. V. Krishnan, and L. Stark, "Optimization of muscle-force sequencing in human locomotion," *Math. Biosci.*, vol. 38, pp. 57–76, 1978.

[3] M. R. Pierrynowski and J. B. Morrison, "Estimating the muscle forces generated in the human lower extremity when walking: A physiological solution," *Mathematics and Bioscience*, vol. 75, pp. 43–68, 1985.

[4] R. D. Crowninshield and R. A. Brand, "A physiologically based criterion of muscle force prediction in locomotion," *J. Biomechan.*, vol. 14, pp. 793–801, 1981.

[5] G. E. Loeb, W. S. Levine, and J. He, "Understanding sensorimotor feedback through optimal control," *Cold Spring Harbor Symposia Quantitative Biol.*, vol. 55, pp. 791–803, 1990.

[6] G. E. Loeb, I. E. Brown, and E. J. Cheng, "A hierarchical foundation for models of sensorimotor control," *Exp. Brain Res.*, vol. 126, pp. 1–18, 1999.

[7] E. Todorov and M. I. Jordan, "Optimal feedback control as a theory of motor coordination," *Nature Neurosci.*, vol. 5, pp. 1226–1235, 2002.

[8] D. Franklin, E. Burdet, R. Osu, M. Kawato, and T. Milner, "Functional significance of stiffness in adaptation of multijoint arm movements to stable and unstable dynamics," *Exp. Brain Res.*, vol. 151, pp. 145–157, 2003.

[9] D. W. Franklin, U. So, M. Kawato, and T. E. Milner, "Impedance control balances stability with metabolically costly muscle activation," *J. Neurophysiol.*, vol. 92, pp. 3097–3105, 2004.

[10] L. Schutte, "Using musculoskeletal models to explore strategies for improving performance in electrical stimulation-induced leg cycle ergometry," Ph.D. dissertation, Stanford Univ., Stanford, CA, 1992.

[11] L. J. Bhargava, M. G. Pandy, and F. C. Anderson, "A phenomenological model for estimating metabolic energy consumption in muscle contraction," *J. Biomechan.*, vol. 37, pp. 81–88, 2004.

[12] B. R. Umberger, K. G. M. Gerritsen, and P. E. Martin, "A model of human muscle energy expenditure," *Comput. Methods Biomechan. Biomed. Eng.*, vol. 6, pp. 99–111, 2003.

[13] N. P. Smith, C. J. Barclay, and D. S. Loisell, "The efficiency of muscle contraction," *Progress Biophys. Mol. Biol.*, vol. 88, pp. 1–58, 2005.

[14] C. J. Barclay, J. K. Constable, and C. L. Gibbs, "Energetics of fast- and slow-twitch muscles of the mouse," *J. Physiol.*, vol. 472, pp. 61–80, 1993.

[15] C. J. Barclay, "Mechanical efficiency and fatigue of fast and slow muscles of the mouse," *J. Physiol.*, vol. 497, pt. 3, pp. 781–794, 1996.

[16] H. Houdijk, M. F. Bobbert, and A. de Haan, "Evaluation of a hill based muscle model for the energy cost and efficiency of muscular contraction," *J. Biomechan.*, vol. 39, pp. 536–543, 2006.

[17] H. Hatze and J. D. Buys, "Energy-optimal controls in the mammalian neuromuscular system," *Biol. Cybern.*, vol. 27, pp. 9–27, 1977.

[18] J. K. Constable, C. J. Barclay, and C. L. Gibbs, "Energetics of lengthening in mouse and toad skeletal muscles," *J. Physiol.*, vol. 505, pt. 1, pp. 205–215, 1997.

[19] M. Linari, R. C. Woledge, and N. A. Curtin, "Energy storage during stretch of active single fibres from frog skeletal muscle," *J. Physiol.*, vol. 548, pp. 461–474, 2003.

[20] G. J. Pinniger, K. W. Ranatunga, and G. W. Offer, "Crossbridge and non-crossbridge contributions to tension in lengthening rat muscle: Force-induced reversal of the power stroke," *J. Physiol.*, vol. 573, pp. 627–643, 2006.

[21] M. Trinh and D. A. Syme, "Effects of stretch on work and efficiency of frog (Rana pipiens) muscle," *J. Exp. Biol.*, vol. 210, pp. 2843–2850, 2007.

[22] R. C. Woledge, C. J. Barclay, and N. A. Curtin, "Temperature change as a probe of muscle crossbridge kinetics: A review and discussion," *Proc. R. Soc. B.*, vol. 276, pp. 2685–2695, 2009.

[23] I. E. Brown, E. J. Cheng, and G. E. Loeb, "Measured and modeled properties of mammalian skeletal muscle. II. The effects of stimulus frequency on force-length and force-velocity relationships," *J. Muscle Res. Cell Mortility*, vol. 20, p. 643, 1999.

[24] I. E. Brown and G. E. Loeb, "Measured and modeled properties of mammalian skeletal muscle: IV. Dynamics of activation and deactivation," *J. Muscle Res. Cell Mortility*, vol. 21, pp. 33–47, 2000.

[25] G. S. Joyce, P. M. H. Rack, and D. R. Westbury, "Mechanical properties of cat soleus muscle during controlled lengthening and shortening movements," *J. Physiol. (London)*, vol. 204, pp. 461–474, 1969.

[26] J. G. Malamud, R. E. Godt, and T. R. Nichols, "Relationship between short-range stiffness and yielding in type-identified, chemically skinned muscle fibers from the cat triceps surae muscles," *J. Neurophysiol.*, vol. 76, pp. 2280–2289, 1996.

[27] W. J. Leijendekker and G. Elzinga, "Metabolic recovery of mouse extensor digitorum longus and soleus muscle," *Pflügers Archiv. Eur. J. Physiol.*, vol. 416, pp. 22–27, 1990.

[28] A. V. Somlyo, H. G. Gonzalez-Serratos, H. Shuman, G. McClellan, and A. P. Somlyo, "Calcium release and ionic changes in the sarcoplasmic reticulum of tetanized muscle: An electron-probe study," *J. Cell Biol.*, vol. 90, pp. 577–594, 1981.

[29] C. J. Barclay, P. D. Arnold, and C. L. Gibbs, "Fatigue and heat production in repeated contractions of mouse skeletal muscle," *J. Physiol.*, vol. 488, pt. 3, pp. 741–752, 1995.

[30] M. T. Crow and M. J. Kushmerick, "Chemical energetics of slow- and fast-twitch muscles of the mouse," *J. General Physiol.*, vol. 79, pp. 147–166, 1982.

[31] I. R. Wendt and C. L. Gibbs, "Recovery heat production of mammalian fast- and slow-twitch muscles," *Am. J. Physiol.*, vol. 230, pp. 1637–1643, 1976.

[32] C. Barclay, R. Woledge, and N. Curtin, "Energy turnover for Ca2+ cycling in skeletal muscle," *J. Muscle Res. Cell Motility*, vol. 28, pp. 259–274, 2007.

[33] C. J. Barclay, G. A. Lichtwark, and N. A. Curtin, "The energetic cost of activation in mouse fast-twitch muscle is the same whether measured using reduced filament overlap or N-benzyl-p-toluenesulphonamide," *Acta Physiol.*, vol. 193, pp. 381–391, 2008.

[34] D. Song, G. Raphael, N. Lan, and G. E. Loeb, "Computationally efficient models of neuromuscular recruitment and mechanics," *J. Neural Eng.*, vol. 5, pp. 175–184, 2008.

[35] N. A. Curtin and R. E. Davies, "Chemical and mechanical changes during stretching of activated frog skeletal muscle," *Cold Spring Harbor Symposia Quantitative Biol.*, vol. 37, pp. 619–626, 1973.

[36] T. M. Butler, N. A. Curtin, and R. E. Davies, "Comparison of ATP usage in muscle during isometric tetanus and activated isovelocity stretch.," *Fed. Proc.*, vol. 31, p. 337, 1972.

[37] T. B. Kelso, D. R. Hodgson, A. R. Visscher, and P. D. Gollnick, "Some properties of different skeletal muscle fiber types: Comparison of reference bases," *J. Appl. Physiol.*, vol. 62, pp. 1436–1441, 1987.

[38] G. Bolstad and A. Ersland, "Energy metabolism in different human skeletal muscles during voluntary isometric contractions," *Eur. J. Appl. Physiol. Occupat. Physiol.*, vol. 38, pp. 171–179, 1978.

[39] G. M. Allen, S. C. Gandevia, and D. K. McKenzie, "Reliability of measurements of muscle strength and voluntary activation using twitch interpolation," *Muscle Nerve*, vol. 18, pp. 593–600, 1995.

[40] E. Saugen and N. K. Vollestad, "Nonlinear relationship between heat production and force during voluntary contractions in humans," *J. Appl. Physiol.*, vol. 79, pp. 2043–2049, 1995.

[41] J. González-Alonso, B. Quistorff, P. Krustrup, J. Bangsbo, and B. Saltin, "Heat production in human skeletal muscle at the onset of intense dynamic exercise," *J. Physiol.*, vol. 524, pp. 603–615, 2000.

[42] P. Andersen, R. P. Adams, G. Sjogaard, A. Thorboe, and B. Saltin, "Dynamic knee extension as model for study of isolated exercising muscle in humans," *J. Appl. Physiol.*, vol. 59, pp. 1647–1653, 1985.

[43] H. Westerblad, J. D. Bruton, and A. Katz, "Skeletal muscle: Energy metabolism, fiber types, fatigue and adaptability," *Exp. Cell Res.*, pp. 3093–3099, 2010.

[44] A. R. Luff and H. L. Atwood, "Changes in the sarcoplasmic reticulum and transverse tubular system of fast and slow skeletal muscles of the mouse during postnatal development," *J. Cell Biol.*, vol. 51, pp. 369–383, 1971.

[45] R. C. Woledge, N. A. Curtin, and E. Homsher, *Energetic Aspects of Muscle Contraction*. London, U.K.: Academic, 1985.

[46] K. E. Jones, A. F. D. Hamilton, and D. M. Wolpert, "Sources of signal-dependent noise during isometric force production," *J. Neurophysiol.*, vol. 88, pp. 1533–1544, 2002.

[47] G. A. Tsianos, G. Raphael, and G. E. Loeb, "Modeling the potentiality of spinal-like circuitry for stabilization of a planar arm system," *Progress Brain Res.*, to be published.
[48] G. J. Van I. Schenau, "From rotation to translation: Constraints on multi-joint movements and the unique action of bi-articular muscles," *Human Movement Sci.*, vol. 8, pp. 301–337, 1989.
[49] S. Gielen, G. Schenau, T. Tax, and M. Theeuwen, "The activation of mono-and bi-articular muscles in multi-joint movements," in *Multiple Muscle Systems: Biomechanics and Movement*, J. Winters and S. Woo, Eds. New York: Springer-Verlag, 1990, pp. 303–311.
[50] R. L. Lieber, "Hypothesis: Biarticular muscles transfer moments between joints," *Dev. Med. Child Neurol.*, vol. 32, pp. 456–458, 1990.
[51] M. G. Pandy and F. E. Zajac, "Optimal muscular coordination strategies for jumping," *J. Biomech.*, vol. 24, pp. 1–10, 1991.
[52] M. Kumamoto, T. Oshima, and T. Yamamoto, "Control properties induced by the existence of antagonistic pairs of bi-articular muscles—Mechanical engineering model analyses," *Human Movement Sci.*, vol. 13, pp. 611–634, 1994.
[53] R. R. Neptune and A. J. Van Den Bogert, "Standard mechanical energy analyses do not correlate with muscle work in cycling," *J. Biomechan.*, vol. 31, pp. 239–245, 1998.
[54] A. C. Schouten, E. de Vlugt, F. C. Van der Helm, and G. G. Brouwn, "Optimal posture control of a musculo-skeletal arm model," *Biol. Cybern.*, vol. 84, pp. 143–152, 2001.
[55] S. A. Kautz, M. L. Hull, and R. R. Neptune, "A comparison of muscular mechanical energy expenditure and internal work in cycling," *J. Biomechan.*, vol. 27, pp. 1459–1467, 1994.
[56] R. M. Enoka and J. Duchateau, "Muscle fatigue: What, why and how it influences muscle function," *J. Physiol.*, vol. 586, pp. 11–23, 2008.
[57] D. G. Allen, G. D. Lamb, and H. Westerblad, "Skeletal muscle fatigue: Cellular Mechanisms," *Physiological Rev.*, vol. 88, pp. 287–332, 2008.
[58] I. E. Brown, T. Satoda, F. J. R. Richmond, and G. E. Loeb, "Feline caudofemoralis muscle: Muscle fiber properties, architecture and motor innervation," *Exp. Brain Res.*, vol. 121, pp. 76–91, 1998.
[59] L. A. Jones and I. W. Hunter, "Effect of fatigue on force sensation," *Exp. Neurol.*, vol. 81, pp. 640–650, 1983.
[60] J. A. Hoffer, N. Sugano, G. E. Loeb, W. B. Marks, M. J. O'Donovan, and C. A. Pratt, "Cat hindlimb motoneurons during locomotion. II. Normal activity patterns," *J. Neurophysiol.*, vol. 57, pp. 530–553, 1987.
[61] K. B. Shelburne and M. G. Pandy, "A musculoskeletal model of the knee for evaluating ligament forces during isometric contractions," *J. Biomechan.*, vol. 30, pp. 163–176, 1997.
[62] J. J. O'Connor, "Can muscle co-contraction protect knee ligaments after injury or repair?," *J. Bone Joint Surg.*, vol. 75-B, pp. 41–48, 1993.
[63] M. G. Hoy, F. E. Zajac, and M. E. Gordon, "A musculoskeletal model of the human lower extremity: The effect of muscle, tendon, and moment arm on the moment-angle relationship of musculotendon actuators at the hip, knee, and ankle," *J. Biomechan.*, vol. 23, pp. 157–169, 1990.
[64] D. M. Pincivero, Y. Salfetnikov, R. M. Campy, and A. J. Coelho, "Angle- and gender-specific quadriceps femoris muscle recruitment and knee extensor torque," *J. Biomechan.*, vol. 37, pp. 1689–1697, 2004.
[65] F. E. Zajac, "Thigh muscle activity during maximum-height jumps by cats," *J. Neurophysiol.*, vol. 53, pp. 979–994, 1985.

George A. Tsianos received the B.S. degree in biomedical engineering with an emphasis in mechanical engineering and the M.S. degree in medical devices and diagnostics engineering, in 2008 and 2009, respectively, from the University of Southern California (USC), Los Angeles, where he is currently working toward the Ph.D. degree.

He was a Research Intern in the Alfred Mann Institute, the University of Southern California (USC), Los Angeles, during 2007 to 2008, where he led the development of a wearable motion tracker for controlling mechatronic prosthetic limbs. He also assisted with quality control of BION injectable neuromuscular stimulators, and development of the BioTac, a biomimetic tactile sensor. Since then, he has been a Research Assistant in the Medical Device Development Facility (MDDF) at USC under the direction of Dr. G. Loeb. His Ph.D. thesis focuses on detailed modeling of muscle physiology and spinal circuitry for understanding how the brain might interact with them to learn and perform motor tasks. He has been funded by the DARPA REPAIR grant and a fellowship from the Myronis Foundation.

Cedric Rustin received the M.S. degree in mechanical engineering from the University of Mons, Mons, Belgium, in 2004. In 2006 he started his doctoral thesis in the Department of Thermics and Combustion, University of Mons, Belgium. His research concerned the physiological modeling and simulation of the human walking and was financed by a grant from the Belgian F.R.S.-FNRS. In this context he spent 10 months in Professor G.E. Loeb's lab in the Department of Biomedical Engineering at the University of Southern California, Los Angeles. He received the Ph.D. degree in engineer sciences in the beginning of 2011.

In 2004, he joined the Department of Thermics and Combustion, University of Mons, Belgium, in order to implement and program simulation methods in thermal radiative transfer. In 2005 he joined the Department of Theoretical Mechanics, Dynamics and Vibration of the same university. During six months he did postgraduate studies in biomechanical modeling. After receiving the Ph.D. degree, he took part in the design of an active orthosis in the framework of the FEDER project named Biomanufacturing. He is currently working for Wow Technology Company which realizes the design, construction, assembly and starting up of tailor-made machines and equipments.

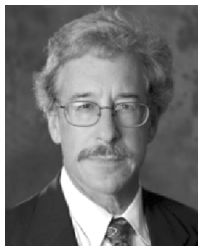

Gerald E. Loeb (M'98) received the B.A. and M.D. degrees from Johns Hopkins University, Baltimore, MD, in 1969 and 1972, respectively.

He did one year of surgical residency at the University of Arizona, Tucson, before joining the Laboratory of Neural Control at the National Institutes of Health, Bethesda, MD (1973–1988). He was Professor of Physiology and Biomedical Engineering, Queen's University, Kingston, ON, Canada (1988–1999) and is now Professor of Biomedical Engineering and Director of the Medical Device Development Facility at the University of Southern California (USC), Los Angeles. He was one of the original developers of the cochlear implant to restore hearing to the deaf and was Chief Scientist for Advanced Bionics Corp. (1994–1999), manufacturers of the Clarion cochlear implant. He is a holder of 52 issued U.S. patents and author of over 200 scientific papers. Most of his current research is directed toward sensorimotor control of paralyzed and prosthetic limbs. His research team developed BION injectable neuromuscular stimulators and has been conducting several pilot clinical trials. They are developing and commercializing a biomimetic tactile sensor for robotic and prosthetic hands through a startup company for which he is Chief Executive Officer. His lab at USC is developing computer models of musculoskeletal mechanics and the interneuronal circuitry of the spinal cord, which facilitates control and learning of voluntary motor behaviors by the brain. These projects build on his long-standing basic research into the properties and natural activities of muscles, motoneurons, proprioceptors, and spinal reflexes.

Dr. Loeb is a Fellow of the American Institute of Medical and Biological Engineers.